Optimal Operating Policies for Tailored Linear Polyethylene Resins Production

K. V. Pontes
LOPCA—Laboratory of Optimization, Design and Advanced Control, Campinas State University, Cidade Universitária Zeferino Vaz, Barão Geraldo, Caixa Postal 1170, Campinas SP, Brazil
PEI—Industrial Engineering Program, Bahia Federal University, R. Aristides Novis n° 2, Federação, Salvador BA, Brazil
AVT—Process Systems Engineering, RWTH Aachen University, Turmstr. 46, 52064, Germany

R. Maciel
LOPCA—Laboratory of Optimization, Design and Advanced Control, Campinas State University, Cidade Universitária Zeferino Vaz, Barão Geraldo, Caixa Postal 1170, Campinas SP, Brazil

M. Embiruçu
PEI—Industrial Engineering Program, Bahia Federal University, R. Aristides Novis n° 2, Federação, Salvador BA, Brazil

A. Hartwich and W. Marquardt
AVT—Process Systems Engineering, RWTH Aachen University, Turmstr. 46, 52064, Germany

DOI 10.1002/aic.11566
Published online July 14, 2008 in Wiley InterScience (www.interscience.wiley.com).

In this work, optimal operating policies for the ethylene polymerization in solution with a Ziegler-Natta catalyst in a series of tubular and stirred tank reactors are proposed. The polymer is specified through properties such as melt index, stress exponent and density. Usually such properties are predicted by means of a process model once the operating conditions are specified. However, the computation of appropriate operating conditions to match desired resins properties is a much more difficult and not yet industrially established task. This problem can be solved through optimization techniques, an efficient alternative to costly pilot plant or production scale tests. A formulation is proposed, where a stationary model of the flowsheet (DAE system) is cast into a multi-stage model with the spatial flow path coordinate as the independent variable. Discontinuities occur at the stage transitions because of model switches and reactants injection. Several studies, involving different polyethylene resin specifications, are carried out to present the high potential and versatility of the suggested procedure. © 2008 American Institute of Chemical Engineers *AIChE J*, 54: 2346–2365, 2008
Keywords: mathematical modeling, optimization, polymerization, simulation, process, design (process simulation)

Introduction

Polyethylene (PE) is a general class of synthetic polymer produced from ethylene. Depending on the type of reactor, the kinetic mechanism and the operating conditions, several

Correspondence concerning this article should be addressed to W. Marquardt at marquardt@lpt.aachen-rwth.de

kinds of PE resins can be produced, with tailored properties to satisfy the requirements of the various final products, including food packing, toys, tubes, or cables. Because of its wide application, PE has replaced materials such as metals, glass or paper, and hence has become an important commodity. Because of the current market competition in thermoplastics industry and worldwide consumption growth, the development of PE resins with even better quality for existing or for new applications is of great interest.

Usually pilot plant or production scale experiments are carried out for this purpose in industry. These industrial scale experiments are indeed empirical correlations between some inlet and outlet variables: the so-called "rules of sum," "short cut calculations," and "trial and error calculations." Obviously such practice does not allow a precise prediction of quality, is time-consuming, results in high costs and most likely leads to off-spec products. Model-based tools constitute an attractive alternative to overcome such disadvantages.

A mathematical process model allows for the prediction of the correlation between process conditions and polymer properties. The evaluation of a process model in a simulation or analysis mode yields the output variables (conversion, polymer properties etc.) for a defined set of input variables (reactant concentrations, reactor configuration etc.) However, when the process model is evaluated in a design or inverse mode to, e.g. determine operating conditions required to produce a resin of prespecified quality, some or all of the input variables have to be determined for specified product qualities. The solution of this inverse problem is much more difficult than the solution of the simulation problem and is not yet an industrially established engineering task. The goal of this work is therefore to develop a method which can efficiently solve the inverse (product design) problem to determine optimal operating policies for continuous ethylene polymerization in order to produce tailored PE resins with specified quality targets. For this purpose, numerical techniques, based on optimal control theory, are tailored to this problem and are applied to an illustrative case study of industrial relevance.

The development of optimal operating policies for polymerization processes has been the subject of a number of previous publications. The present contribution focuses on continuous polymerization processes, whereas most other authors have studied batch polymerization. Louie and Soong,[1] Chen and Lee,[2,3] Ponnuswamy et al.,[4] Choi and Butala,[5] Vaid and Gupta,[6] and Tieu et al.,[7] for example, minimize the batch time while satisfying prespecified polymer properties and monomer conversion at the end of the batch. Conversely, Secchi et al.,[8] Ahn et al.,[9] and Hanai et al.[10] do not consider the minimization of the batch time, but define the deviation of the conversion and the polymer properties from the required value as objective of the optimization. Chakravarthy et al.[11] and Oliveira et al.[12] minimize a multiobjective function consisting of batch time and this deviation. Ray and Gupta,[13] Srivastava and Gupta,[14] and Scali et al.[15] maximize or minimize a specific polymer property, whereas the values of all other properties are maintained at a fixed value. Ray and Gupta,[13] Brandolin et al.,[16] Zhou et al.,[17] Faliks et al.,[18] Lemoine-Nava and Flores-Tlacuahuac[19] improve reactor performance by maximizing conversion and constraining the polymer properties.

Obviously maximum conversion or minimum batch time are related to higher revenues or lower cost, but these objectives do not ensure optimal operation from an economical point of view. Only few authors employ an economic objective accounting for operational cost. O'Driscoll and Ponnuswamy,[20] Tieu et al.[7] and Oliveira et al.[12] consider the initiator cost together with the batch time in a multi-objective optimization, the constraints of which account for polydispersity (PD), molecular weight, and copolymer composition (when it applies).

All cited contributions have formulated an optimization problem in order to determine optimal operating policies to reach a resin of specified quality. Another approach, though less frequently used, employs neural networks to find an inverse model. For example, Fernandes et al.[21] have developed a neural network to obtain an inverse model for the vinyl-acetate batch emulsion polymerization. For given polymer properties (molecular weight, PD, particle diameter, and branching frequency) and reactor productivity, the neural network determines the operating conditions of the polymerization. The inverse neural network modeling of Curteanu[22] yields reaction conditions (temperature and initial initiator concentration), which assure certain values of conversion and polymerization degree at the end of the batch. Within this scope, there is also the contribution of Gosden et al.,[23] who predict the instantaneous reactor feed conditions for a specified product MWD applied to a continuous stirred tank reactor (CSTR).

Modeling of ethylene polymerization has vastly been studied in literature. There are plenty of contributions approaching free radical polymerization.[24–26] In the field of coordination polymerization with a Ziegler-Natta catalyst the majority of studies focus on the gas phase process.[27–29] There are additionally some studies on slurry polymerization.[30–31] In fact only few contributions have addressed the ethylene polymerization process in solution with a Ziegler-Natta catalyst, which is approached in the present case study. For example, Kim and Choi[32] and Cozewith[33] investigate the steady-state and transient behavior of ethylene copolymers in a CSTR with a soluble Ziegler-Natta catalyst. Additionally, Embiruçu et al.[34] analyze the ethylene polymerization in a train of CSTR and PFR (plug flow reactor) and Hinchliffe et al.[35] develop a hybrid model for a dual CSTR, with a soluble Ziegler-Natta catalyst as well. To the authors' knowledge, solely Brandolin et al.[16] address the problem of determining optimal operating policies to achieve certain resin properties for ethylene polymerization. However, they treat a free radical mechanism in a continuous high pressure tubular reactor. They derive optimal operating policies (temperature and initiator concentration) in order to attain a specific number average molecular weight, PD, and weight average branch point number in the effluent product.

As one can see, the modeling of ethylene polymerization with soluble catalyst or even the optimal design of operating conditions have rarely been addressed in literature. Besides, the consideration of economic aspects in the objective function and the use of polymer properties (melt index, stress exponent and density) as constraints are still rare. Although optimal operating policies for batch polymerization reactors have been addressed by several authors, the determination of optimal operating conditions for ethylene polymerization

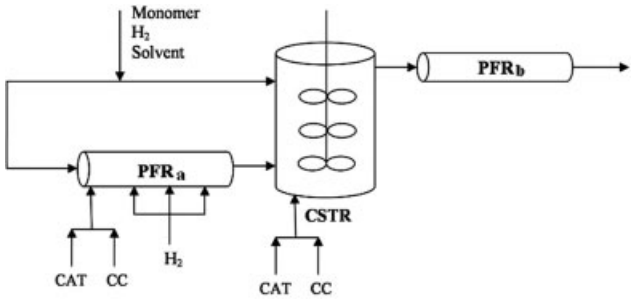

Figure 1. Polymer reactor system.

with soluble catalyst in a continuous process still needs more attention.

The present study suggests the formulation and solution of a new kind of optimization problem to find optimal operating conditions to produce polymer resins with prespecified properties for the ethylene polymerization in solution with a Ziegler-Natta catalyst in a train of CSTR and PFR reactors. At first, the process used as a case study is described. Then, the mathematical models of the polymerization process and the polymer properties are given. In the next section an optimization problem based on optimal control theory for multistage systems is formulated. Following, several optimal operating policies for tailored polymer grades are obtained from the model to illustrate the applicability and potential of the proposed procedure. Finally, the article is concluded.

Process Description

The polymerization process under consideration is a real industrial case study and consists of three reactors, two PFR, and one CSTR, according to Figure 1. The two types of reactors comprise different residence time distributions and spatial temperature and concentration profiles because of their inherent fluid dynamic characteristics. Hence, each type of reactor contributes in a different way to the resulting molecular weight distribution (MWD) of the polymer product. For example, the polymer produced in a PFR has a broader MWD compared to the polymer that is produced in a CSTR.

The sample reactor configuration in Figure 1 can be operated in very different ways to produce a large variety of polymer grades. Varying the injection point of the catalyst/co-catalyst mixture or the stirring of the agitator in the CSTR, the resulting reactor characteristics can vary from that of a single almost ideal CSTR to a single tubular reactor and any intermediate characteristic as well. When both PFR and the CSTR are employed, the resulting resin reflects the characteristics of both reactor types and shows properties varying from a very narrow to a very broad MWD. The possibility of several process configurations makes this reactor system very attractive for the prediction of a variety of product grades. Two possible configurations most frequently used in industrial practice are chosen for illustration of the proposed approach and are detailed as follows:

- In the tubular configuration (Figure 2, left), the agitator in the CSTR is switched off, such that it operates as a PFR with a large diameter resulting in some degree of back-mixing due to axial dispersion. The catalyst/co-catalyst mixture is injected at the inlet of the tubular reactor to start the reaction. Chain transfer agent (hydrogen) can not only be added in the feed but also at several points along PFR_a in order to control the MWD.
- In the stirred configuration (Figure 2, right), the catalyst/co-catalyst mixture is injected only at the bottom of the CSTR, where the reaction is started. In this case, PFR_a does not function as a reactor, but solely as a feeder to the CSTR. The main feed can be split and part of it enters at the top of the CSTR. A higher side feed rate results in a lower feed rate at the bottom. When the mixture is entering PFR_b, the reaction is almost completed.

In industrial practice it is also possible to add comonomer to produce a linear low density polyethylene (LLDPE). However, the greater production share consists of homopolymer or copolymer with just a small content of comonomer. Therefore, previous studies have focused on modeling the homopolymerization process and validating the model with actual industrial data.[34,36] Hence, the present study addresses the homopolymerization process, which produces linear polyethylene (LPE), because a validated model is available.

The catalyst is a mixture of vanadium- and titanium-based catalysts, activated by triethyl aluminum. The kinetic mechanism is described by the following reactions[34,37]:

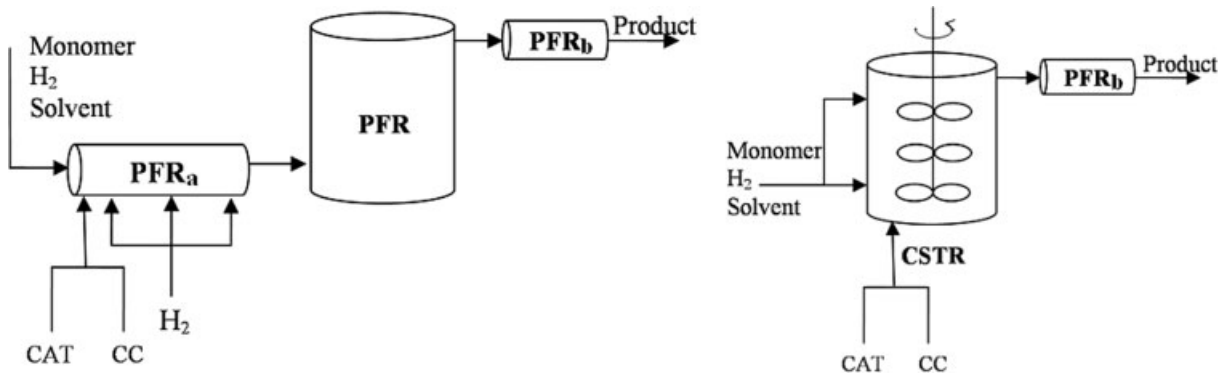

Figure 2. Typical configuration: tubular (left) and stirred (right).

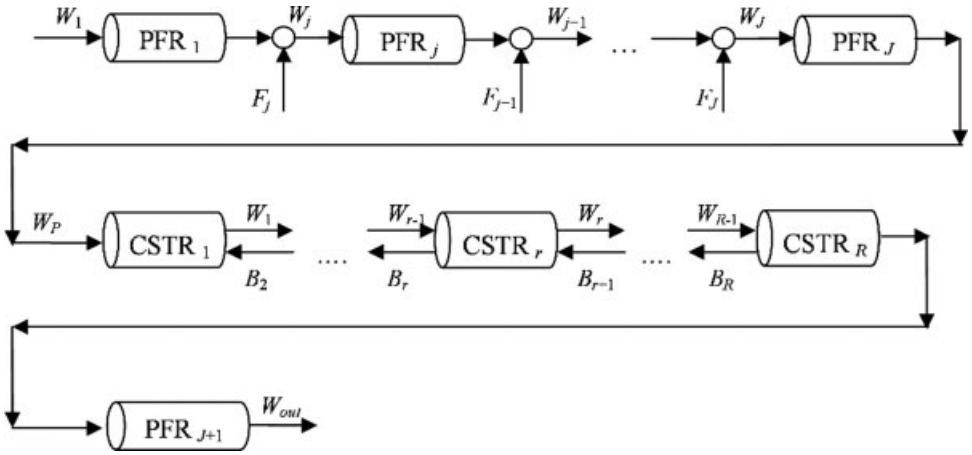

Figure 3. Model structure for the tubular configuration.

Activation:

$$\mathrm{CAT}_n + \mathrm{CC} \xrightarrow{k_{f',n}} C_n^*$$

Poisoning:

$$I_{\mathrm{CC}} + \mathrm{CC} \xrightarrow{k_{icc'}} \mathrm{CCD}$$

$$I_{\mathrm{C}^*} + C_n^* \xrightarrow{k_{ic^*,n}} \mathrm{CD}_n$$

Initiation:

$$C_n^* + M \xrightarrow{k_{i,n}} P_{1,n}$$

Propagation:

$$P_{p,n} + M \xrightarrow{k_{p,n}} P_{p+1,n} \quad p = 1, 2, 3, \ldots, \infty$$

Transfer:

$$P_{p,n} + M \xrightarrow{k_{fm,n}} P_{1,n} + U_{\mathrm{p}}$$

$$P_{p,n} + H_2 \xrightarrow{k_{fh,n}} C_n^* + U_{\mathrm{p}}$$

$$P_{p,n} + \mathrm{CC} \xrightarrow{k_{fCC,n}} C_n^* + U_{\mathrm{p}}$$

$$P_{p,n} \xrightarrow{k_{f,n}} C_n^* + U_{\mathrm{p}}$$

Deactivation:

$$C_n^* \xrightarrow{k_{d,n}} \mathrm{CD}$$

Termination:

$$P_{p,n} + M \xrightarrow{k_{tm,n}} \mathrm{CD} + U_{\mathrm{p}}$$

$$P_{p,n} + H_2 \xrightarrow{k_{th,n}} \mathrm{CD} + U_{\mathrm{p}}$$

$$P_{p,n} + \mathrm{CC} \xrightarrow{k_{tCC,n}} \mathrm{CD} + U_{\mathrm{p}}$$

$$P_{p,n} \xrightarrow{k_{t,n}} \mathrm{CD} + U_{\mathrm{p}}$$

CAT refers to catalyst, CC to co-catalyst, C^* to the active species, I_{C} to a catalyst poison, I_{CC} to a co-catalyst poison, CCD to the co-catalyst deactivated by poisoning, CD to the deactivated catalyst, H_2 to hydrogen, M to monomer, P_p to live polymer with p monomer units and U_p to dead polymer with p monomer units. The subscript n corresponds to active species, according to the active site multiplicity theory.[38]

Process Model

Since both reactor system configurations described above have their particular mathematical model and input variables, each one is treated separately throughout this article. The degrees of freedom and the results are analyzed individually. Before the mathematical model of the process is presented, the fundamental modeling assumptions and the modeling concept are discussed. The tubular and stirred configurations represented in Figure 2 are modeled according to Figures 3 and 4, respectively.

For the tubular configuration (Figure 3), $\mathrm{PFR_a}$ is divided into J segments with PFR characteristics, where the starting point of compartment j is located at the lateral mass injection points (F_{j}). In the stirred configuration (Figure 4), the nonideal CSTR is represented by a sequence of R ideally mixed compartments in series with back-mixing (B) between two adjacent compartments to represent the mixing inside the reactor.[34,39–41] Additionally, the side feeds to the CSTR are represented by FZ_r.

For each PFR segment, the total and component mass balances for the steady-state model are given by

$$W_{j+1} = F_{j+1} + W_j \quad j = 1, 2, \ldots J, \tag{1}$$

$$\frac{1}{A}\frac{dW_j}{dz_j} = 0 \Leftrightarrow W_j = \text{constant}, \tag{2}$$

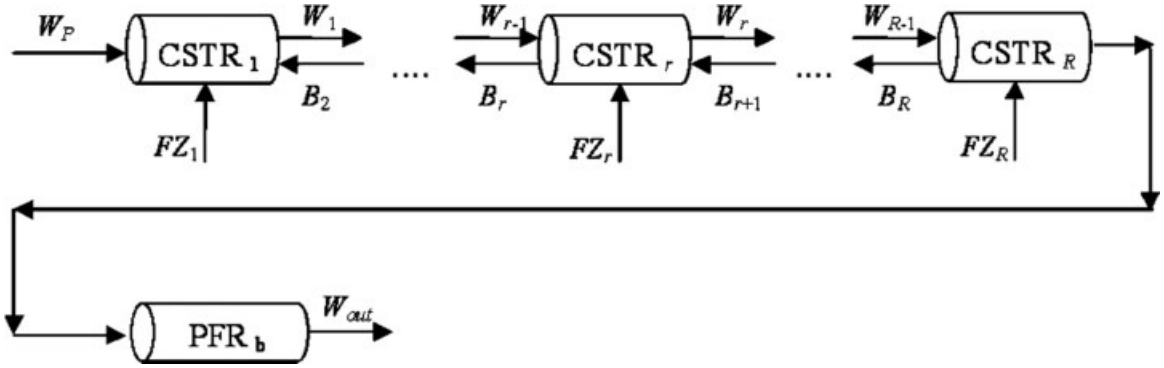

Figure 4. Model structure for the stirred configuration.

$$\frac{dC_{i,j}}{dz_j} = \frac{C_{i,j}}{\rho_j} \cdot \frac{d\rho_j}{dz_j} + r_i \cdot \frac{A.\rho_j}{W_j}, \quad z_j \in (0, l_j], \tag{3}$$

with initial conditions

$$\begin{aligned} W_j(z_j = 0) &= W_{0,j}, \\ C_{i,j}(z_j = 0) &= C_{0,i,j}, \\ \rho_j(z_j = 0) &= \rho_{0,j}, \end{aligned} \tag{4}$$

where z is the axial coordinate, l_j is the length of segment j, W_j and F_j are mass flow rates (kg/s), $C_{i,j}$ is the concentration of component i (kmol/m^3), r_i is the reaction rate of component i (kmol/s m^3), A is the cross-sectional area (m^2), and ρ is the density of the mixture (kg/m^3). Equation 2 implies that the mass flow rate is constant in every tubular reactor segment.

Since the stirred tank reactor is modeled by several ideal CSTR compartments, the total and component mass balances for each compartment (r) in steady-state are

$$W_{r-1} + FZ_r + B_{r+1} - B_r - W_r = 0 \quad r = 1, \ldots, R, \tag{5}$$

$$\begin{aligned} \frac{W_{r-1} \cdot C_{i,r-1}}{\rho_{r-1}} + \frac{FZ_r \cdot C_{i,r}}{\rho_{\mathrm{FZ}_r}} + \frac{B_{r+1} \cdot C_{i,r+1}}{\rho_{r+1}} \\ - \frac{(B_r + W_r) \cdot C_{i,r}}{\rho_r} + V_r \cdot r_{i,r} = 0, \\ B_1 = 0, \\ B_{R+1} = 0, \\ W_0 = W_j, \end{aligned} \tag{6}$$

where B_r, FZ_r, W_r are the mass flow rates (kg/s), $C_{i,r}$ is the concentration of component i (kmol/m^3), $r_{i,r}$ is the reaction rate of component i (kmol/s m^3), V_r is the volume (m^3), and ρ_r is the mixture density (kg/m^3). The last equation states that the inlet flow rate to the first CSTR zone is equal to the outlet flow rate of the last segment of PFR$_a$; therefore, it applies only for the tubular configuration.

The mixing inside the stirred tank reactor is represented by the back-mixing stream between the ideal compartments. The empirical model used here is adopted from Embiruçu et al. (2000)[34]; it assumes that mixing is due to the inherent dispersion, the action of the mechanic agitator and the lateral feed. The back-mixing stream is modeled as

$$B_r = \frac{k \cdot \rho_r \cdot V_r}{\mu_r} \cdot \left(D_{0,r} + D_{\mathrm{Rot},r} \cdot \mathrm{Rot} + D_{\mathrm{F},r} \cdot \frac{FZ_r}{\sum_{r=1}^{\mathrm{nr}} FZ_r + W_1} \right), \tag{7}$$

where k is a proportionality coefficient, μ is the viscosity of the solution, D_0, D_{Rot}, and D_{F} are empirical constants, Rot is the energy input of the agitator and FZ is the side feed rate.

The energy balances for each reactor are developed taking into account the following assumptions:

- potential and kinetic energies and the agitator work are neglected;
- the system is adiabatic, as observed in industrial practice;
- the volume of one CSTR segment is constant;
- the specific heat of the polymer is independent of the chain length;
- heat effects of the polymerization reactions other than the propagation reaction may be neglected, since heat is mainly generated by propagation.

Hence, the energy balances for the CSTR and PFR (see Appendix for a derivation) read as

$$\begin{aligned} \sum_i W_i \int_{T^r}^{T^i} Cp_i dT = -V \cdot r_{\mathrm{p}} \\ \times \left(\Delta \overline{\mathrm{H}}_{\mathrm{p}}^o + \mathrm{MW}_{\mathrm{M}} \cdot \int_{T^o}^{T^r} (C\mathrm{p}_{\mathrm{U}} - C\mathrm{p}_{\mathrm{M}}) dT \right), \\ i \in [FZ_r, W_{r-1}, B_{r+1}], \end{aligned} \tag{8}$$

$$\begin{aligned} \frac{W_j}{A} \cdot \frac{dT_j}{dz_j} = -\frac{r_{\mathrm{P}}}{C\mathrm{p}} \cdot \left(\Delta H_{\mathrm{p}}^o + \mathrm{MW}_{\mathrm{M}} \cdot \int_{T^o}^{T^r} (C\mathrm{p}_{\mathrm{U}} - C\mathrm{p}_{\mathrm{M}}) dT \right), \\ j = 1, \ldots, J, \end{aligned} \tag{9}$$

respectively, where $C\mathrm{p}_{\mathrm{U}}$ and $C\mathrm{p}_{\mathrm{M}}$ are the specific heat (J/kg · K) of polymer and monomer, MW_{M} is the molecular weight of the monomer (kg/kmol), r_{p} is the reaction rate of the propagation (kmol/s m^3), ΔH_{p}^o is the enthalpy of this reaction at the reference temperature (J/kmol), T^r is the reaction temperature, T^i is the input temperature and T^o is the reference temperature. The initial conditions of Eq. 9 are

$$T_j(z_j = 0) = T_0, \quad j = 1, \ldots, J. \tag{10}$$

The assumption of an adiabatic process is justified because possible energy losses due to nonideal isolation as well as the agitator work are small and can therefore be neglected. The model does not account for heaters or coolers upstream and downstream the reactor. Therefore, the energy for heating the inlet streams or cooling the outlet streams can not be predicted by the model.

The moments of the MWD are defined according to

$$\lambda_k = \sum_{p=1}^{\infty} p^k \cdot U_p, \quad k = 0, 1, 2, \tag{11}$$

where the index k defines the moment order and p is the number of monomer units in the dead polymer chain with concentration U. This definition can be applied to the component mass balance Eqs. 3 and 6 in order to calculate the first three moments λ_0, λ_1, λ_2. These quantities allow for the evaluation of the numerical and weight average molecular weights, $\overline{\mathrm{MW}}$, and $\overline{\mathrm{MW}}_w$, and the PD through the equations

$$\overline{\mathrm{MW}}_n = \mathrm{MW_M} \cdot \frac{\lambda_1}{\lambda_0}, \tag{12}$$

$$\overline{\mathrm{MW}}_w = \mathrm{MW_M} \cdot \frac{\lambda_2}{\lambda_1}, \tag{13}$$

$$\mathrm{PD} \equiv \frac{\overline{\mathrm{MW}}_w}{\overline{\mathrm{MW}}_n}, \tag{14}$$

where $\mathrm{MW_M}$ is the molecular weight of the monomer.

The quality of the polymer is determined through properties such as melt index (MI), stress exponent (SE), and density (DS), which can be correlated to the average molecular weights ($\overline{\mathrm{MW}}_n$ and $\overline{\mathrm{MW}}_w$ and to PD.

The melt index (MI) is defined as the amount of polymer (weight) extruded during a 10-min test at specified conditions, and is thus inversely related to the average molecular weight.[42] An empirical model to represent the melt index reported in literature[28,34,43–45] and widely used in industrial practice, is given by

$$\mathrm{MI} = \alpha_1 \cdot \left(\overline{\mathrm{MW}}_w\right)^{-\beta_1}, \tag{15}$$

where α_1 and β_1 are empirical constants.

The stress exponent (SE) is another property considered in industrial practice to verify the polymer quality. It measures the non-Newtonian behavior of the polymer and is defined by

$$\mathrm{SE} = \frac{\log\left(\mathrm{MI}[3p] \Big/ \mathrm{MI}[p]\right)}{\log 3}, \tag{16}$$

where p is the weight used in the standard MI test, MI[p] is the melt index measured in the standard test configuration while MI[$3p$] is the melt index evaluated when applying a weight three times higher ($3p$) than the standard weight during the test. If SE equals unity, viscosity does not change when a higher weight is employed; therefore, the fluid shows Newtonian behavior. This property indicates the broadness of the MWD and also correlates with PD. The empirical correlation

$$\mathrm{SE} = \frac{1}{\alpha_2 + \gamma_2 \cdot \exp(-\beta_2 \cdot \mathrm{PD})}, \tag{17}$$

reported by Embiruçu et al.[34] is adopted here, where α_2, β_2, and γ_2 are empirical constants. The stress exponent SE is proportional to the PD, i.e., a high PD also means a high SE and vice-versa.

The polymer density (DS) is mostly affected by the comonomer content, since it introduces branches to the linear polymer chain.[28] For the ethylene homopolymerization considered here, the correlation

$$\mathrm{DS} = \alpha_3 + \beta_3 \cdot \log(\mathrm{MI}) + \gamma_3 \cdot \mathrm{SE} - \delta \cdot [\mathrm{CM}]^{\varepsilon}, \tag{18}$$

proposed by Embiruçu et al.[34] is used. It considers not only comonomer content (CM), but also the influence of the molecular weight MW and PD, via melt index MI and stress exponent SE, on the polymer density, though with a smaller effect than that of the comonomer composition.

Reactor conversion Q and polymer production rate $\mathrm{W_{PE}}$ are given by

$$\mathrm{Q} = 100 \cdot \frac{\lambda_1}{C_M + \lambda_1}, \tag{19}$$

$$\mathrm{W_{PE}} = \frac{W}{\rho} \cdot \lambda_1 \cdot \mathrm{MW_M}, \tag{20}$$

respectively, where C_M is the monomer concentration, W the total mass flow rate, $\mathrm{MW_M}$ is the monomer molecular weight and ρ the mixture density. They should be accounted for to assess process performance.

The viscosity of a polymer solution is generally higher than that of the solvent, even at low polymer concentrations: it increases with increasing molecular weight.[46] Therefore, the pressure drop is predominantly determined by the viscosity of the polymer, which is obtained by the Mark-Houwink correlation,[42]

$$\mu = \tau \cdot \left(\overline{\mathrm{MW}}_w\right)^{\xi}, \tag{21}$$

where μ is the polymer viscosity and τ and ξ are empirical constants.

A rigorous momentum balance, which determines the pressure drop along the reactor, is not included in the model because previous experimental studies[47] have shown that the simplified pressure drop model

$$\Delta P = K \cdot \mu \cdot W_{\mathrm{PE}}^2 \tag{22}$$

can satisfactorily predict the process behavior. K is a proportionality constant and μ is the polymer viscosity, for which the Mark-Houwink correlation is used (Eq. 21). The pressure drop is computed for each PFR and CSTR segment to account for viscosity variation along the reactor length.

The kinetic and physical parameters are adopted from Embiruçu et al.,[34] who modeled the same ethylene polymer-

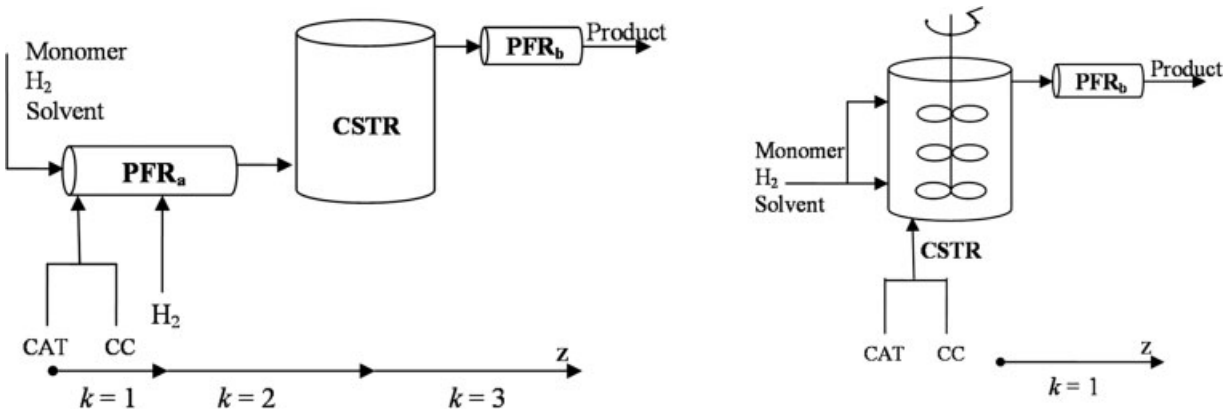

Figure 5. Stages (*k*) definition along the axial coordinate: tubular (left) and stirred (right).

ization process. They develop a methodology to fit the model predictions with the actual dynamic plant data, which covered the production of 15 different polymer grades. The MI and SE were used to validate the MWD through estimation of the empirical constants in Eqs. 15, 17, 18, 21, and 22. The numerical strategy combines data reconciliation procedures and standard parameter estimation techniques to filter the operational data sets and to improve the performance of the estimation process.[36] Embiruçu et al.[34] show that the estimated parameters allow for a satisfactory prediction of the experimental industrial data.

Optimization Problem—Mathematical Description

The stationary mathematical model of the CSTR presented in Process Model is formed only of algebraic equations, whereas the PFR model is formed by a system of ordinary differential equations (an ODE system) with the axial coordinate z being the independent variable. Since boundary conditions are only stated at the inlet, the resulting initial value problem may be solved by integrating along the axial coordinate z.

Many chemical engineering models display discontinuities along the independent coordinate caused by either physical changes or external actions and disturbances affecting the process. Thus, the process behavior may be described by a sequence of stages separated by so-called events such as reactant feed along a tubular reactor or a change in the mathematical model. For example, the model describing the process shown in Figure 1 displays discontinuities due to a mass injection along PFR_a. Such a process model can be interpreted to be of multistage type.[48–50] More precisely, the model of the tubular configuration in Figure 3 is of multistage type with complicated stage transition conditions. In particular, the set of algebraic equations representing the series of CSTR maps the outlet conditions of PFR_J to the initial conditions of PFR_{J+1}. Both of these PFR are associated with a finite length spatial interval and hence are modeled by differential-algebraic equations. In contrast, each CSTR may be associated with a zero length spatial interval and represented by an algebraic model. If one hydrogen injection point is considered, the tubular configuration comprises three stages, i.e. two compartments of PFR_a and PFR_b while the CSTR is modeled by few compartments that map the variables between PFR_a outlet and PFR_b inlet. When employing the stirred configuration of Figure 4, the model comprises only one stage, i.e. PFR_b. The inlet conditions of $CSTR_1$ are mapped to the inlet condition of PFR_b by the models of the sequence of CSTR. The resulting multi-stage systems for the tubular and the stirred configurations are graphically depicted in Figure 5 for convenience.

Multi-Stage Optimization Problem

Optimization of steady-state operation of the polymerization process results in an optimization problem with differential-algebraic equality and possible additional inequality constraints. Hence, algorithms and software for the solution of dynamic optimization or optimal control problems can readily be applied if the independent coordinate is interpreted to be the spatial coordinate.

For the problem addressed, it is desired to define the operating conditions in order to produce a prespecified polymer, described by properties such as MI, SE, and DS. Several operating conditions may yield similar resins, but one of them may be the best from an economical point of view. Hence, the optimization problem may be formulated as determining suitable operating policies to produce a resin with tailored properties at maximum profit. The objective function is then given by

$$\Phi = a \cdot W_{PE} - (b_M \cdot W_M + b_H \cdot W_H + b_{CAT} \cdot W_{CAT} + b_{CC} \cdot W_{CC} + b_S \cdot W_S)\ €/s, \quad (23)$$

where a is the polyethylene sales price (€/kg), b_j represent the cost (€/kg) of raw material j, W are mass flow rates and the subscripts PE, M, H, CAT, CC, and S denote polyethylene, monomer, hydrogen, catalyst, co-catalyst, and solvent, respectively. Energy and other cost could be considered in a more comprehensive and complete economic objective function.

The product quality specifications correspond to the polymer properties at the outlet of PFR_b in both configurations. These properties can be specified within a tolerance range or

Table 1. Efficiency of Computation[a]

	Stirred Configuration		Tubular Configuration	
	Example 2a	Example 3c	Example 5b	Example 4a
Differential variables	12	12	47	47
Algebraic variables	1698	1698	1929	1929
Decision variables	7	7	7[b]	8
Transition conditions	12	12	36	36
NLP iterations	93	44	140	81
CPU time (s)	486	100	1242	418

[a]Execution in 2.0 GHz AMD Atlon 64 Processor 3200+.
[b]z_1 is fixed to a pre-defined value, then it does not constitute a decision variable.

by a nominal value resulting in (end-point) inequality or equality constraints at the end of PFR_b, i.e., at $z = z_f$. Additional operational constraints may exist for the decision variables, such as the applicable maximum or minimum of the reactant inlet concentrations, of the total mass flow rate, inlet temperature or pressure. In addition, the system pressure and temperature should be kept within bounds everywhere in order to guarantee that only one phase exists.

For both, the tubular and the stirred configurations, the degrees of freedom to be determined by the optimization include the inlet concentrations of monomer (M), hydrogen (H_0) and catalyst (CAT), the inlet temperature (T_{in}), the total mass flow rate (W_t) and the inlet pressure (P_{in}). In case of the stirred configuration, the side feed (W_s) to the CSTR constitutes an additional decision variable. Some peculiarities also apply for the tubular configuration. Since it is possible to inject hydrogen along the tubular reactor at different points, the locations z_j and the hydrogen concentration H_j, $J = 1, \ldots, J - 1$ are additional decision variables. Hence, the vectors of decision variables for the stirred and tubular configurations are given by $\mathbf{u}_s$ and $\mathbf{u}_t$ as follows:

$$\mathbf{u}_s = [\,\mathrm{M} \quad \mathrm{H_0} \quad \mathrm{CAT} \quad \mathrm{T_{in}} \quad \mathrm{W_s} \quad \mathrm{W_t} \quad \mathrm{P_{in}}\,]^T, \tag{24}$$

$$\mathbf{u}_t = [\,\mathrm{M} \quad \mathrm{H_0} \quad \mathrm{CAT} \quad \mathrm{T_{in}} \quad \mathbf{H} \quad \mathbf{z} \quad \mathrm{W_t} \quad \mathrm{P_{in}}\,]^T, \tag{25}$$

where $\mathbf{H} = [\mathrm{H}_1 \cdots \mathrm{H}_{J-1}]^{\mathrm{T}}$ and $\mathbf{z} = [z_1 \cdots z_{J-1}]^T$.

It is important to point out that the total reactor length is held constant, such that

$$z_{L_a} = \sum_{i=0}^{J} z_i, \;\; z_0 = 0, \tag{26}$$

where z_{L_a} is the total length of PFR_a and J is the number of PFR segments. The number of hydrogen lateral feed points is

Table 2. Polyethylene Sales Price and Raw Material Cost

	Value (€/kg)
a	0.90
b_{M}	0.55
b_{H}	300
b_{CAT}	700
b_{CC}	200
b_{S}	0.02

Table 3. Initial Guesses and Bounds of the Controls—Stirred Configuration

	IG	LB	UB
CAT	0.436	0.256	0.641
M	0.925	0.625	1.000
H_0	0.500	0.033	1.000
T_{in}	0.000	0.000	0.364
P_{in}	0.385	0.000	0.846
W_t	0.400	0.200	0.600
W_s	0.222	0.111	0.667

defined a priori, in such a manner that any discrete variable is considered in the model.

Since the R compartments of the nonideal CSTR do not constitute a stage but solely an algebraic mapping condition between the stages represented by the PFR, the stages of the stirred and the tubular configurations may be grouped into the sets

$$\xi_s = \{1\}, \quad \xi_t = \{1, \ldots, J, J+1\}, \tag{27}$$

where the subscripts s and t indicate the stirred and the tubular configuration, respectively, and where ξ refers to all the stages in the specified configuration. The optimal control problem may then be formulated as

$$\max_{\mathbf{u}} \Phi \tag{28}$$

s.t.

$$\dot{\mathbf{x}}_k = \mathbf{f}_k(\mathbf{x}_k, \mathbf{y}_k, \mathbf{u}_k, \mathbf{p}_k, z), \; z \in [z_{k-1}, z_k], \; k \in \xi_s \vee \xi_t, \tag{28a}$$

$$0 = \mathbf{g}_k(\mathbf{x}_k, \mathbf{y}_k, \mathbf{u}_k, \mathbf{p}, z), \; z \in [z_{k-1}, z_k], \; k \in \xi_s \vee \xi_t, \tag{28b}$$

$$0 = \mathbf{x}_1(z_0) - \mathbf{x}_0, \;\; \text{tubular configuration}, \tag{28c}$$

$$\mathbf{J}_1(\dot{\mathbf{x}}_1, \mathbf{x}_1, \mathbf{y}_1, \mathbf{u}_1, \dot{\mathbf{x}}_0, \mathbf{x}_0, \mathbf{y}_0, \mathbf{u}_0, \mathbf{p}, 0) = \mathbf{0}, \;\; \text{stirred configuration}, \tag{28d}$$

$$\mathbf{J}_k(\dot{\mathbf{x}}_k, \mathbf{x}_k, \mathbf{y}_k, \mathbf{u}_k, \dot{\mathbf{x}}_{k-1}, \mathbf{x}_{k-1}, \mathbf{y}_{k-1}, \mathbf{u}_{k-1}, \mathbf{p}, z) = \mathbf{0}, \; k \in \xi_t \backslash \{1\}, \tag{28e}$$

$$\mathbf{u}_{i,\mathrm{LB}} \le \mathbf{u}_i \le \mathbf{u}_{i,\mathrm{UB}}, \; i = \mathrm{s\,or\,t}, \tag{28f}$$

$$\mathrm{MI_{LB}} \le \mathrm{MI} \le \mathrm{MI_{UB}}, \quad z = z_f, \tag{28g}$$

$$\mathrm{SE_{LB}} \le \mathrm{SE} \le \mathrm{SE_{UB}}, \quad z = z_f, \tag{28h}$$

$$\mathrm{DS_{LB}} \le \mathrm{DS} \le \mathrm{DS_{UB}}, \quad z = z_f, \tag{28i}$$

Table 4. Example 1—Stirred Configuration

Example	1a	1b	1c	1d	1e
MI	0.294	0.294	0.294	0.294	0.294
SE	0.260	0.270	0.280	0.290	0.300

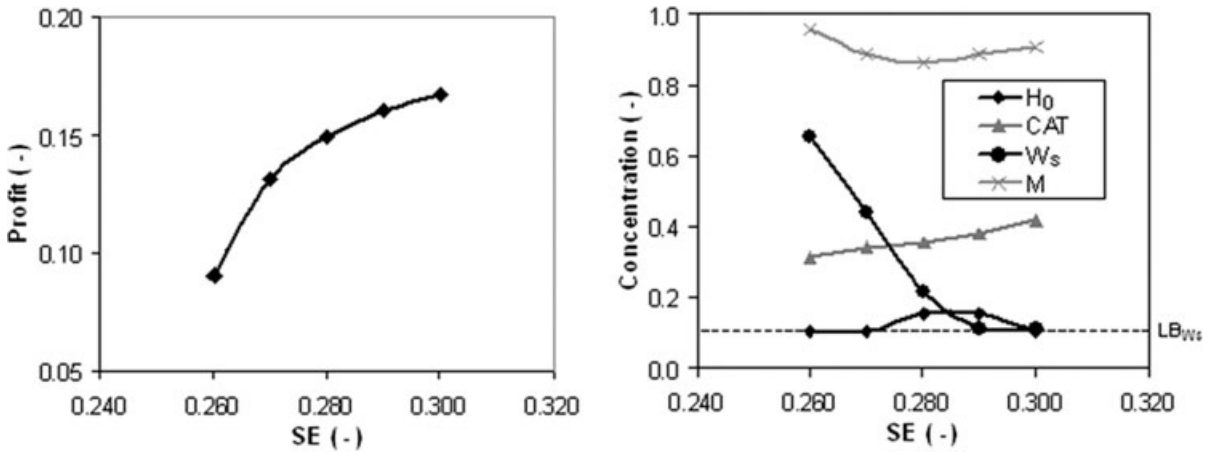

Figure 6. Example 1: Profit vs. SE (left); reactant concentrations vs. SE (right). MI = 0.294.

$$T_{out,LB} \leq T_{out} \leq T_{out,UB}, \quad z = z_f, \tag{28j}$$

$$P_{out,LB} \leq P_{out} \leq P_{out,UB}, \quad z = z_f, \tag{28k}$$

where k denotes a specific stage, $\mathbf{x}$ are differential state variables, $\mathbf{y}$ the algebraic state variables, $\mathbf{u}$ the decision variables (defined by Eqs. 24 and 25), $\mathbf{p}$ the invariant parameters, z the axial coordinate and the indices s and t indicate the stirred and tubular configuration, respectively. The coordinate z is chosen such that the spatial coordinate of stage k runs from z_{k-1} to z_k. Note, that the spatial coordinate does not progress in the stirred tank reactors, because a compartment modeling approach is chosen.

For the tubular configuration, the differential equations 28a are valid on the stages represented by PFR models and correspond to component mass balance and energy balance, Eqs. 3 and 9, respectively. The algebraic equations 28b are formed by the total mass balance Eqs. 1 and 2 and also by the polymer properties and outlet variables such as conversion and polymer production rate. The initial conditions of PFR_a, 4 and 10, are set by 28c, where $\mathbf{x}_0$ is the initial condition and $\mathbf{x}_1$ the state variables of stage $k = 1$. For the following PFR segments $k = [2, \ldots, J + 1]$, the initial conditions are determined by the mapping conditions (28e). The CSTR model does not comprise any differential equations, but only algebraic such as Eqs. 5, 6, 7, and 8, besides the polymer properties correlations. Hence, the CSTR model is independent of the spatial domain and the according equations can be incorporated into the mapping conditions (28e).

Analogously to the tubular configuration, the CSTR model in the stirred configuration, represented by Eqs. 5, 6, 7, and 8 and by the polymer properties correlations is given by the mapping condition $\mathbf{J}_1$ (Eq. 28d). It maps the initial conditions for the first stage, i.e. PFR_b.

Implementation

The multistage process model, that calculates the polymer properties given the inlet conditions, has been developed in the commercial simulator gPROMS (General Process Modeling System). The optimization is carried out by means of DyOS,[51–52] a software tool for the solution of dynamic optimization problems, developed and maintained at AVT,

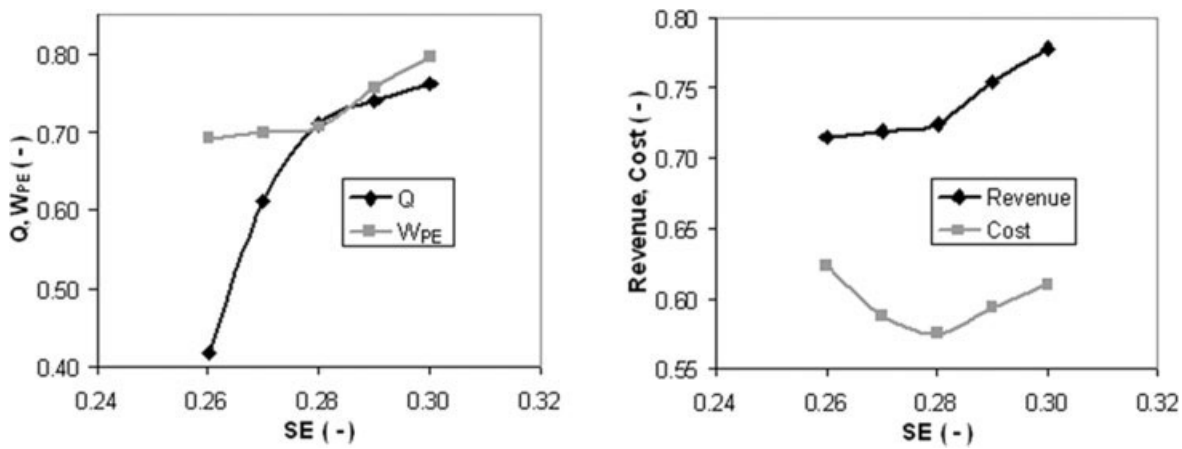

Figure 7. Example 1: Conversion (Q) and polymer production rate (W_{PE}) vs. SE (left); revenue and cost vs. SE (right). MI = 0.294.

Table 5. Example 2—Stirred Configuration

Example	2a	2b	2c	2d	2e	2f
MI	0.201	0.235	0.294	0.353	0.412	0.471
SE	0.300	0.300	0.300	0.300	0.300	0.300

Process Systems Engineering, RWTH Aachen University, Germany. DyOS solves the dynamic optimization problem numerically by an adaptive sequential (or single-shooting) approach.[53] The solution of the resulting nonlinear program is accomplished by the package SNOPT.[54] The sensitivities for the computation of the gradients are solved by a highly efficient semi-implicit extrapolation method tailored to the characteristic properties of the sensitivity system.[55] The availability of such sophisticated dynamic optimization tool facilitates the application of the suggested approach.

The computational time required for the optimization varied from 1.5 to 20 min, depending on the model (stirred or tubular configuration) and the polymer property specifications. Table 1 presents the statistics on the computation of some results presented in the next section. A fast and a slow optimization run are selected for both reactor configurations.

Examples 2a and 5b required significantly more computational time in comparison to Examples 3c and 4a to solve the optimization problem. The strict endpoint constraints on the polymer properties pose an additional challenge to the NLP solver. Furthermore, the performance of the computations depends on the initial guess for the decision variables.

Results and Discussion

Several optimization studies are carried out considering different polymer resin specifications for both reactor configurations. The data shown here reflect an actual industrial case study and are therefore normalized for confidentiality reasons according to

$$v_n = \frac{v - v_{\min}}{v_{\max} - v_{\min}}, \tag{29}$$

where the indices max and min indicate maximum and minimum limits, n refers to the normalized values and v represents all variables shown in the results, such as the controls, control bounds and initial guesses, the polymer properties and the output variables. Because of this normalization all variables are dimensionless.

Arbitrary, but qualitatively coherent values are employed for polyethylene sales prices and raw material cost, according to Table 2. In the following tables and plots, IG refers to the initial guesses and LB and UB to the lower and upper bounds of the optimization. The lines in all figures connect the computed sample points for better visualization. They do not correspond to computational results. Not all the decision variables in Eqs. 24 and 25 are illustrated in the plots, but only the ones which present significant changes at the optimum.

Stirred configuration

For the stirred configuration, lower and upper bounds, as well as the initial guesses for the controls are summarized in Table 3. The polymer properties are also defined a priori, but, since they are specific for each example, their values will be given individually.

In Example 1, a sequence of specifications with varying stress exponent SE for a constant melt index MI is evaluated. In Example 2, another sequence of optimizations is carried out, where several MI values are specified and the SE is maintained at a constant value. Example 3 is similar to the previous one, but a lower SE is specified in order to compare the results to those of Example 2. It is worth highlighting that the PD is proportional to SE; therefore, the observed SE tendencies also apply for PD.

Example 1. In Example 1, the specified polymer properties are depicted in Table 4. The results are illustrated in Figures 6 and 7.

According to the backmixing model discussed previously in Eq. 7, the side feed ensures a proper mixing inside the reactor. Therefore, a more homogeneous resin, with a lower SE is produced. For this reason, one can observe in Figure 6 (right) that the side feed (W_s) vanishes towards higher values for SE. Besides, higher catalyst concentrations (CAT) lead to

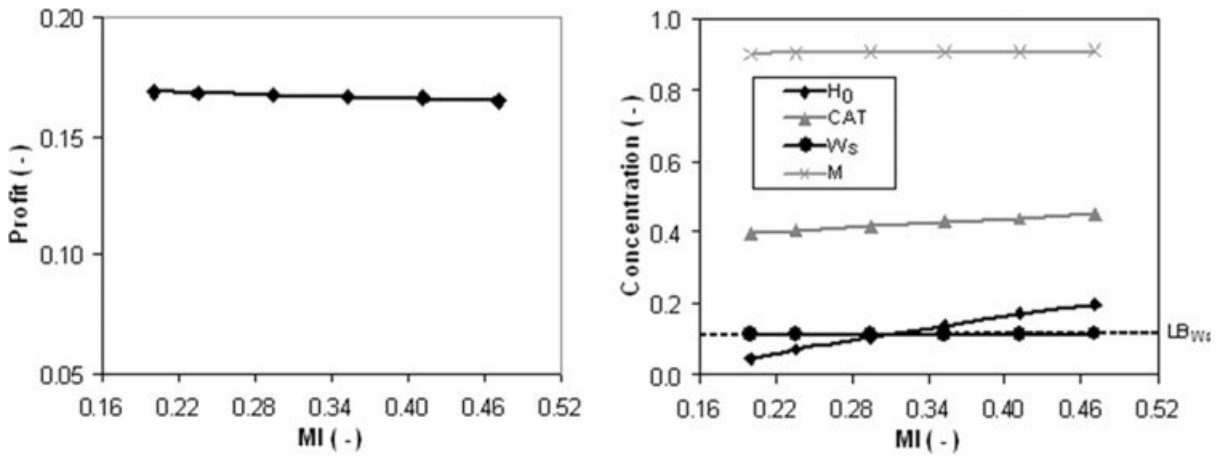

Figure 8. Example 2: Profit vs. MI (left); reactant concentrations vs. MI (right). SE = 0.300.

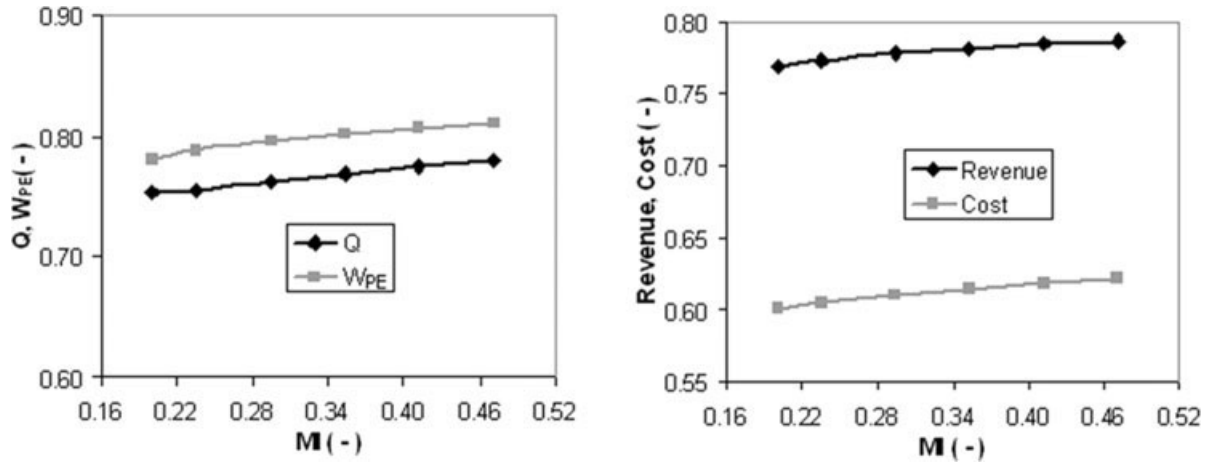

Figure 9. Example 2: Conversion (Q) and polymer production rate (W_{PE}) vs. MI (left); revenue and cost vs. MI (right). SE = 0.300.

higher SE values. For a more detailed discussion of the phenomena taking place inside the reactor, for example how the catalyst influences SE or MI, the reader is referred to Embiruçu et al.[34]

Some of the trends observed in Figure 6 (right) tend to reduce the MI while others tend to increase it. Therefore, the simultaneous occurrence of these trends must result in a compensation effect in order to attain the constant MI specification. According to Figure 2 (right), the side feed results from a split of the main feed. Hence, lower values of the side feed rate result in higher flow rates at the bottom of the CSTR. Thereby, a larger amount of polymer of high molecular weight and lower MI is produced in the first sections of the CSTR. Therefore, the observed decrease in the side feed, Figure 6 (right), could reduce the polymer MI. On the other hand, the observed increase in the hydrogen and catalyst concentrations, as well as the decrease in ethylene concentration, act in the opposite way and increase the MI. The global effect is then the constant MI as specified. However, when W_s reaches its lower bound (at SE = 0.290), represented by the dashed line in Figure 6 (right), it cannot impact SE anymore. Consequently, a decrease of the hydrogen input concentration (H_0) and an increase of the ethylene input concentration (M) are observed to ensure higher values for SE.

In Figure 6, the catalyst and ethylene inlet concentrations vary respectively from −28 to −4% and from +4 to −2% of the initial guesses, respectively (Table 3). Therefore, a low MI associated with the lowest specified SE requires a very low catalyst and a high ethylene concentration. This diminishes conversion, due to the catalyst deactivation effect (see the kinetic model),[34] and, consequently, polymer production rate and revenues, while leading to higher production costs (Figure 7). The lowest profit results for the lowest SE specified, followed by a rapid increase because of the reduction in the ethylene consumption.

Example 2. For Example 2, the specified polymer properties are shown in Table 5 and the optimization results are presented in Figures 8 and 9.

Unlike in Example 1, the side feed values are at the lower bound (LB_{Ws}), represented by the dashed line in Figure 8 (right). This can be associated with the higher SE required in Example 2, since lower side feeds tend to increase the value of this property. The increasing catalyst (CAT) and hydrogen (H_0) concentrations observed in Figure 8 (right) assure higher MI values as specified. On the other hand, the SE is maintained at the desired constant value because catalyst and hydrogen have opposite effects on this property. Higher catalyst and ethylene concentrations lead to greater revenues due to increasing conversion and polymer production rate (Figure 9). However, the cost increases more rapidly resulting in lower profits towards higher values of MI. In Figure 8, the catalyst and ethylene inlet concentrations vary from −8 to 17% and from −3 to −0.7% of the initial guesses, respectively (Table 3).

Example 3. The specified polymer properties of Example 3 are depicted in Table 6. In analogy to the previous example, a sequence of MI is studied. However, a more homogeneous polymer with SE = 0.260 is specified here. The results are shown in Figures 10 and 11.

When comparing Figures 8 and 10, it is worth noting that the lower SE required in Example 3 leads to lower profits, but with an increasing tendency towards higher MI. As discussed before, when low values of SE and MI are combined, very low amounts of catalyst and, consequently, high amounts of ethylene are required. This leads to low conversion and high costs for the reactants (Figure 11). As the required MI increases, the catalyst concentration also increases, allowing for a lower consumption of monomer (Figure 10, right). As a consequence, higher conversion is achieved whereas the polymer production rate, and hence the revenue are maintained at a constant level (Figure 11, left). Therefore, savings of raw material (ethylene) can be related to the observed increase in profit (Figure 10).

Table 6. Example 3—Stirred Configuration

Example	3a	3b	3c	3d	3e	3f
MI	0.294	0.353	0.412	0.471	0.529	0.588
SE	0.260	0.260	0.260	0.260	0.260	0.260

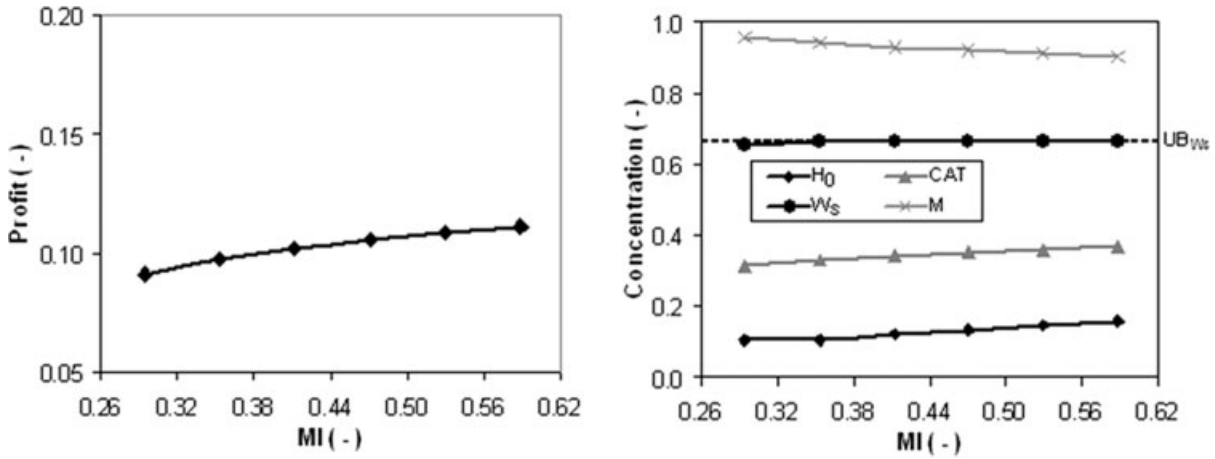

Figure 10. Example 3: Profit vs. MI (left); reactants concentrations vs. MI (right). SE = 0.260.

It is also worth to highlight that the side feed values are at the upper limit, UB_{Ws} (represented by a dashed line in Figure 10, right), unlike Example 2 (Figure 8, right), since a lower SE is required here.

Discussion of Results

All the optimizations reveal that the total mass flow rates (W_t) are at the upper limit. This can be associated with the fact that a higher total mass flow rate leads to a larger polymer production, thus guaranteeing higher incomes.

It is important to emphasize the nonlinear behavior of the process. For increasing MI, the profit can increase or decrease, depending on the required SE. Examples 2 and 3 above illustrate that lower SE values yield lower profits, but with an increasing profile towards higher MI, unlike the more elevated SE values. Figure 6 is in accordance with Figures 8 and 10, that is, higher SE values allow higher profit; however, the rate of profit increase tends to get smaller (Figures 6 and 10) or even becomes negative (Figure 8). As mentioned before, the side feed to the CSTR (W_s) is the most important variable to control the SE, followed by the catalyst inlet concentration (CAT). Hence, when W_s reaches its bounds and can not manipulate SE anymore, the catalyst concentration is the variable of choice. Higher catalyst inlet concentrations enhance SE (or PD), MI, and conversion. Lower ethylene inlet concentration reduces SE but, on the other hand, increases MI and diminishes the deactivation effect due to the lower temperatures. Therefore, for resins with lower SE (Example 3), a decrease in ethylene concentration may be observed towards increasing MI (Figure 10, right). This decreasing behavior of the ethylene concentration allows for lower operational costs and less pronounced catalyst deactivation since the operational temperatures are lower. On the other hand, for higher SE values (Example 2), the ethylene concentration is not allowed to assume lower values towards higher MI (Figure 8, right). The increasing operational costs then can not compensate the higher revenues, resulting in lower profits towards higher MI values (Figure 9, right; Figure 8, left). Therefore, the nonlinear behavior of the process reflected in the SE is a trade-off between catalyst/conversion and ethylene/deactivation effects.

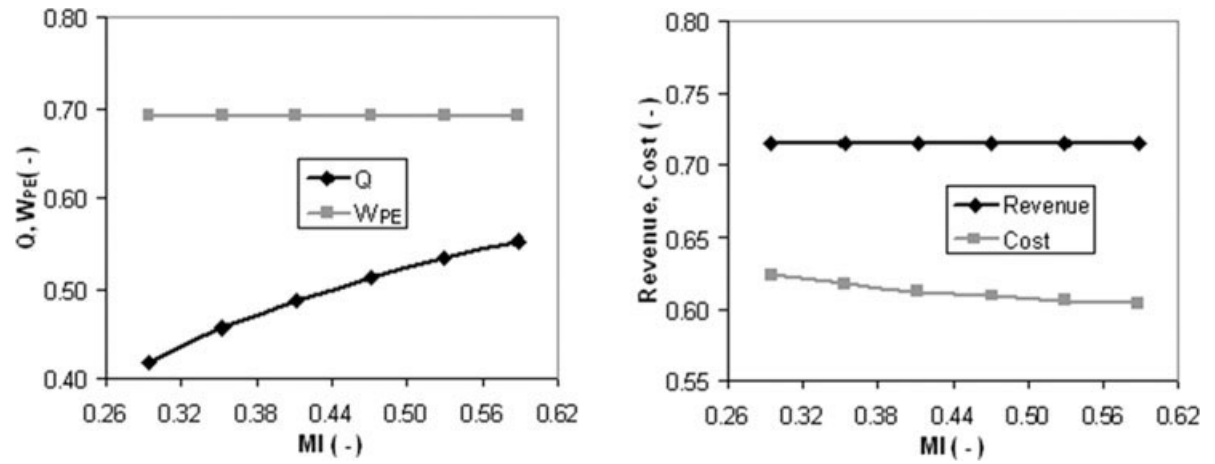

Figure 11. Example 3: Conversion and polymer production rate vs. MI (left); revenue and cost vs. MI (right). SE = 0.260.

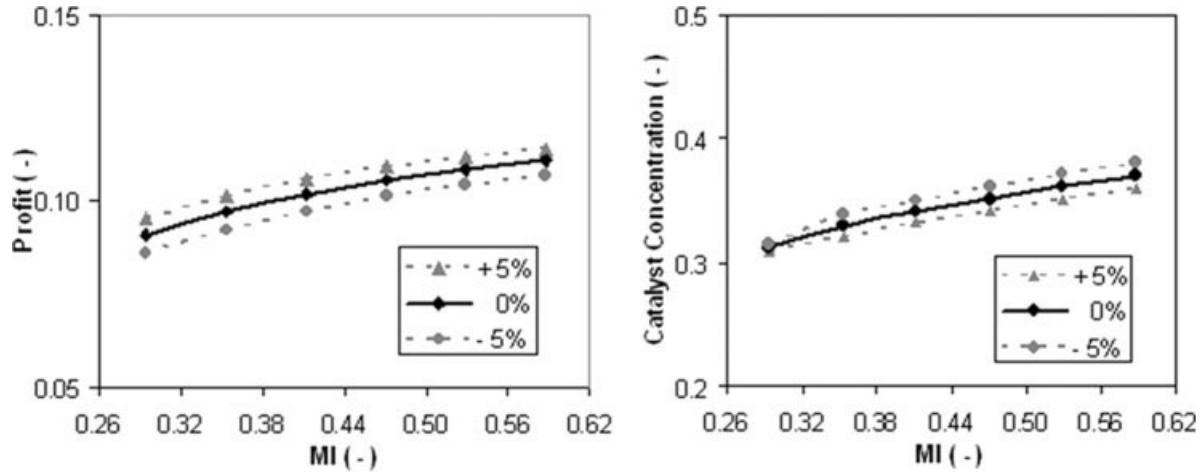

Figure 12. Change from −5 to +5% in the Arrhenius constant of the propagation reaction.

The optimization procedure developed here allows for a simple and skilled generation of data, allowing an easy identification of the process nonlinearity, a task that would be very laborious when based only on process knowledge and on pilot plant or production scale experiments. For that reason, this optimization can bring improvements to the process operation and to the design of products with better quality.

As discussed previously, the kinetic and physical parameters have been taken from literature. The qualitative aspects discussed above are in accordance with the analysis of Embiruçu et al.[34] However, a question that may arise is how the parametric uncertainty can influence the results obtained. A detailed analysis is out of scope of this work, but a brief assessment will be given next. Figure 12 illustrates the results for a change of the Arrhenius constant of the propagation reaction from −5 to +5%, respectively. The trends of all responses are the same and the observed quantitative differences are less expressed. However, when applying this optimization model in an industrial environment, an appropriate model fitting and model validation is mandatory, since small differences in profit, as the ones observed in Figure 12, can represent a large impact on the economics.

Tubular configuration

For the tubular configuration, the initial guesses for the controls and the corresponding bounds are summarized in Table 7. Along the first tubular reactor one hydrogen injection point is considered, hence $J = 2$, $\mathbf{H} = [H_1]$ and $\mathbf{z} = [z_1]$.

Table 7. Initial Guesses and Bounds of Controls—Tubular Configuration

	IG	LB	UB
CAT	0.742	0.677	1.000
M	0.708	0.625	0.833
H_0	0.112	0.017	0.333
T_{in}	0.375	0.250	1.000
P_{in}	0.692	0.538	1.000
W_t	0.600	0.400	1.000
H_1	0.568	0.018	0.855
z_1	0.351	0.144	0.434

Three examples are studied for the tubular configuration. First, the MI, SE, and DS of the polymer are specified within a certain tolerance interval. As in Example 1, a sequence of optimizations is carried out, where several SE values are specified for constant MI. In the last example, the result of the optimization is compared with actual industrial practice.

Before a discussion of the results, it is worthwhile to explain some peculiarities of the process in more detail. The hydrogen is the chain transfer agent, i.e., it reduces the polymer molecular weight and increases the MI through the transfer reactions with the live polymer chains. Therefore, it is proportional to MI and plays an important role in the control of this property. Besides, when more hydrogen is fed and smaller chains, with higher MI, are produced, the polymer tends to be more homogeneous, resulting in lower values for SE. As mentioned previously, another very important variable for the control of MI and, mainly, of SE, is the location of the second hydrogen injection point and the respective feed concentration. The hydrogen as a chain transfer agent triggers a discontinuity in the reactor profile at the injection point; the polymer tends to be more heterogeneous downstream. The longer the distance between the reactor inlet and the first hydrogen injection point (z_1), the more heterogeneous (higher SE) the produced polymer will be. This can be related to the fact that the produced resin is a mixture of polymers produced in each reactor region and a considerable amount of dead polymer already exists at higher values of z_1. Obviously, higher hydrogen concentrations at that point enhance this effect. When the hydrogen is injected closer to the reactor inlet (lower z_1), it contributes more to the transfer reactions, consequently increasing MI. To clarify this relationship, an overview of this discussion is summarized in Table 8, where the symbol (+) indicates that an increase in the control variables leads to an increase of the property value whereas (−) leads to a decrease.

Table 8. Effects of Chain Transfer Agent on MI and SE

Controls	MI	SE
H_0	(+)	(−)
H_1	(+)	(+)
z_1	(−)	(+)

Table 9. Effect of the Upper Bound of the Outlet Temperature

Variable			Optimum		
Type	Name	IG	$T_{out,max}$ 1.000	$T_{out,max}$ 0.900	$T_{out,max}$ 0.800
Design variable	CAT	0.742	0.845	0.837	0.828
	M	0.708	0.751	0.728	0.702
	H_0	0.112	0.026	0.017	0.017
	T_{in}	0.375	0.250	0.250	0.250
	P_{in}	0.692	1.000	1.000	1.000
	W_t	0.600	0.400	0.469	0.556
	H_1	0.568	0.150	0.187	0.219
	z_1	0.351	0.322	0.290	0.311
Quality variable	MI	0.425	0.226	0.224	0.224
	SE	0.621	0.700	0.700	0.700
	DS	0.924	0.924	0.924	0.924
Output variable	T_{out}	0.866	1.000	0.900	0.800
	P_{out}	0.265	0.500	0.500	0.500
	Q	0.963	0.970	0.974	0.978
	W_{PE}	0.590	0.570	0.568	0.568
	Revenue	0.654	0.642	0.641	0.641
	Cost	0.561	0.530	0.533	0.537
	Profit	0.094	0.113	0.108	0.104

Example 4. This optimization study aims to produce a PE resin with the following properties:

$$0.224 \leq \text{MI} \leq 0.228,$$
$$0.700 \leq \text{SE} \leq 0.704, \quad (30)$$
$$0.920 \leq \text{DS} \leq 0.928.$$

The operating conditions at the initial guess and at the optimum are summarized in Table 9 for three different upper bounds of the outlet temperature $T_{out,max}$. The total mass flow rate (W_t) reaches its lower bound for $T_{out,max} = 1.0$, whereas the inlet pressure (P_{in}) is located at its upper bound. This can be associated with the fact that lower MI, i.e., higher molecular weight and higher viscosity, leads to a higher pressure drop.

Another active constraint, besides the W_t and P_{in}, is the outlet temperature, which is active at its upper limit. A sequence of optimizations has been carried out to investigate the effect of the upper bounds of the outlet temperature on the optimal profit. The results are given in the following columns of Table 9 for $T_{out,max} = 0.9$ and $T_{out,max} = 0.8$.

Increasing monomer and catalyst concentrations result in higher propagation reaction rates and consequently higher temperatures. Therefore, lower optimal input concentrations are observed when the maximum outlet temperature is reduced. Despite the lower ethylene concentration, the revenue is maintained at nearly the same level due to the higher total mass flow rate (W_t). But, on the other hand, the production cost increases. As a consequence, decreasing profit is observed. Therefore, the outlet temperature constraint plays an important role on the profit. It is interesting to highlight the different hydrogen concentrations and locations of the injection point among the three cases. These decision variables have no major effect on the temperature, conversion or polymer production rate, but are adjusted in order to attain the required polymer properties, while ethylene and catalyst ensure higher profits.

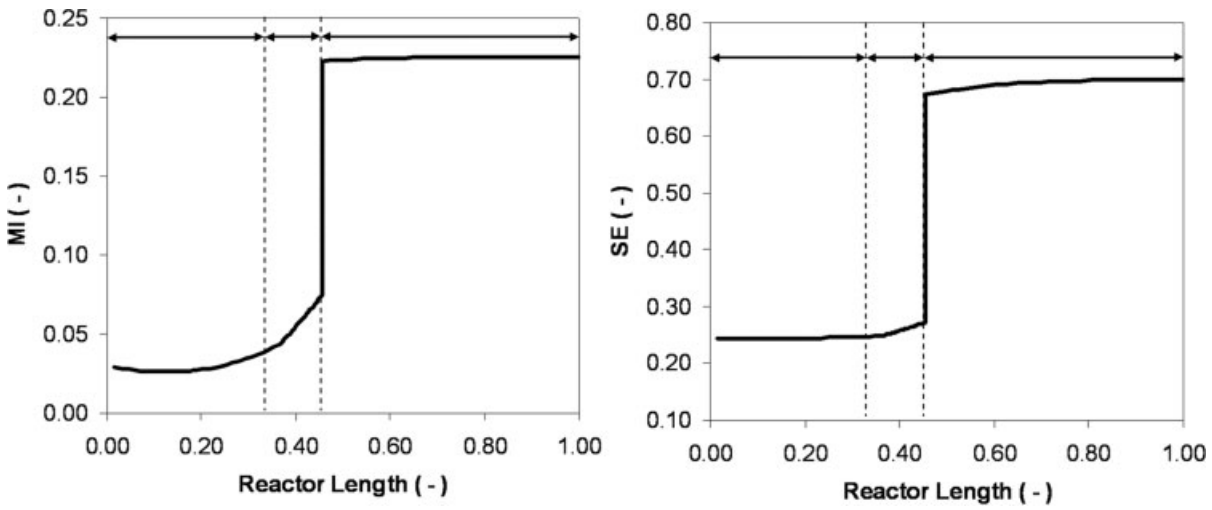

Figure 13. MI and SE profiles along the reactor—tubular configuration. $T_{out,max} = 1.000$.

Table 10. Example 5—Tubular Configuration

Example	5a	5b	5c	5d	5e	5f
MI	0.565	0.565	0.565	0.565	0.565	0.565
SE	0.456	0.500	0.550	0.600	0.650	0.700

Figure 13 illustrates the MI and SE profiles along the reactor length for Example 4 with $T_{out,max} = 1.0$, where the dashed lines and the arrows delimit the stages. In the first PFR, there is the first discontinuity because of the injection of hydrogen at $z_1 = 0.322$, since it changes the state of the system. The second discontinuity corresponds to a switch of reactors, i.e., the end of the first tubular reactor and the beginning of the CSTR, followed by the beginning of the last tubular reactor; the mathematical model is switched. These profiles then illustrate the multistage feature of the process studied.

The PFR is a distributed parameter system, unlike the CSTR, which is homogeneous. Hence, when the reacting mixture enters the CSTR, the reaction conditions change greatly and abruptly, for example, there is a great temperature increase from the outlet of the first PFR to the inlet of the first CSTR zone. As a result the polymer properties also change greatly and abruptly. Therefore, the CSTR operation has much more influence in the polymer properties than the location of hydrogen side feed, as shown in Figure 13.

Example 5. The next example specifies resins with the properties given in Table 10. The hydrogen injection point along PFR_a reactor was fixed at $z_1 = 0.33$. The results are illustrated in Figures 14 and 15, where LB_{CAT} and UB_{CAT} indicate the lower and upper bounds of the catalyst inlet concentration.

The degrees of freedom that change the most are catalyst and hydrogen concentrations (Figure 14, right). Higher catalyst (CAT) and lower hydrogen concentrations at the inlet (H_0) lead to an increase in SE and in production costs. Since a constant MI is specified, an increasing hydrogen concentration (H_1) at the injection point is observed, since the catalyst and H_0 responses would decrease the MI. The slightly decreasing ethylene concentrations associated with an increasing catalyst concentration lead to higher conversions whereas to an almost constant polymer production rate and revenue (Figure 15). As a consequence, lower profits are obtained when higher values of SE are required for a constant MI (Figure 14, left).

The tendency of the PFR to produce polymer resins with broader MWD and higher SE values has been discussed previously. This claim can be supported when one compares the stirred configuration results (Figure 7) with those of the above example. Besides, when the tubular configuration is employed, the temperature is lower at the reactor inlet and increases along the reactor length. On the other hand, in a CSTR, the temperatures inside this reactor are much higher. Since higher temperatures enhance transfer, termination, and deactivation reactions, the molecular weight of the polymer produced in a CSTR is lower. For this reason, the tubular configuration allows for the production of resins with lower MI.

When comparing Figure 14 to Figure 6, one can note the opposite behavior of profit on SE for the tubular and the stirred configurations, indicating once more the high nonlinearity of the process studied and the importance and usefulness of the proposed procedure.

Example 6—industrial practice. To compare the model developed with the current industrial practice, a resin with MI = 0.282, SE = 0.713, and DS = 0.925 is taken as a reference case. Its operational conditions are summarized in Table 11. The output variables are calculated by the process model. An optimization is then carried out in order to determine the optimal operating policy to produce a polymer with the same properties and higher profit. The lower and upper bounds are adopted from Table 7 and the initial guesses are set to the operating condition used in industry. The result is presented as Scenario 1 in Table 11. A higher profit can be obtained not only due to lower costs but also due to higher revenues. This indicates that the operating point used in industrial practice is clearly a sub-optimal. Usually, the market demands certain amounts of resin grades, which are specified by the production planning; hence a new optimization is carried out next, constraining the polymer production

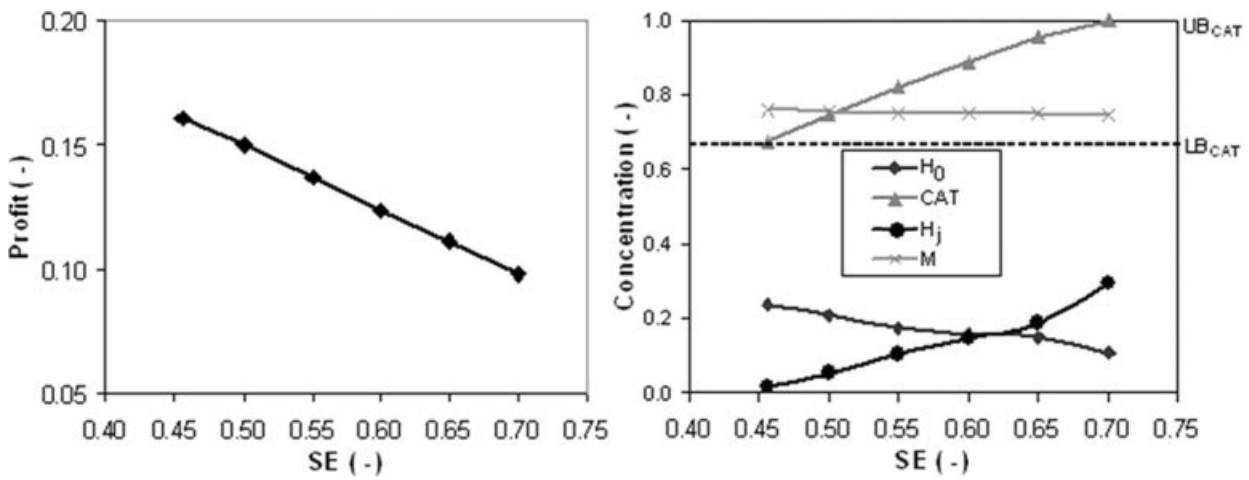

Figure 14. Example 5: Profit vs. SE (left); reactants concentrations vs. SE (right). MI = 0.565.

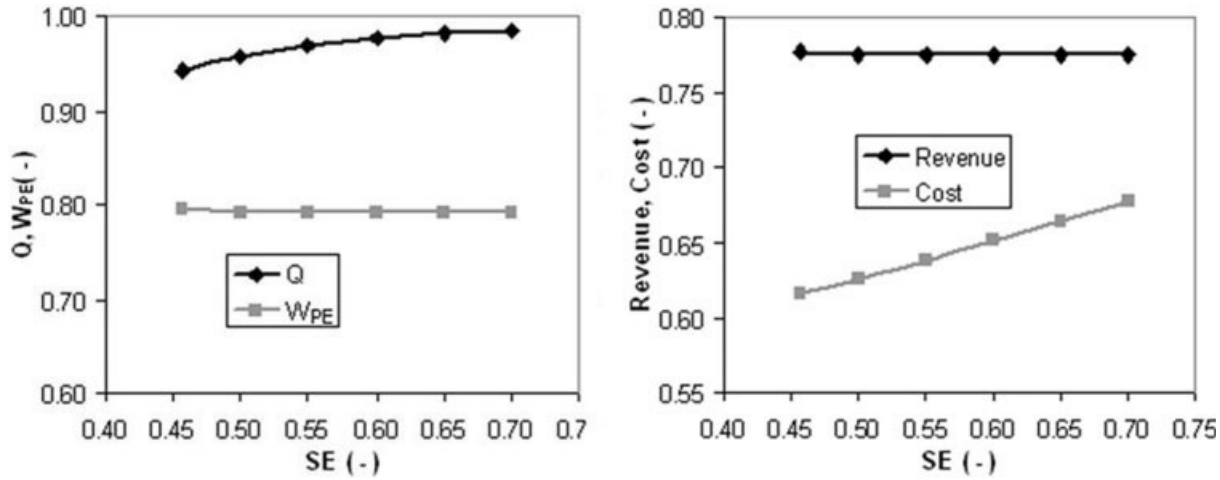

Figure 15. Example 5: Conversion and polymer production rate vs. SE (left); income and cost vs. SE (right). MI = 0.565.

rate to $W_{PE} = 0.605$ as in the industrial reference case. The results, shown as Scenario 2 in Table 11, show the new optimal operating policy. Despite the lower profit, there is still a significant improvement when compared to the reference case. These results illustrate that the proposed approach can not only contribute to a much better economical performance of the process but can also be used to adjust plant operation to changing demands on product quality. In the example studied, a significant improvement of about 20% can be reached.

Conclusions

This article presents a novel optimization approach to deal with the determination of optimal operating policies for the production of tailored products in continuous polymerization. The polymerization process selected as a case study can produce different kinds of polyethylene depending on the operating conditions. This operational flexibility is also due to the presence of two types of reactors (tubular and stirred tank) in series, different side feed injection points of the chain transfer agent (hydrogen) and utilizations of different reactor configurations. The steady-state process is represented by a multistage model to account for the combination of different reactors and different positions of the hydrogen injection along the reactor. It is given by a set of continuous/discrete differential-algebraic equations with the axial coordinate as the independent variable. Therefore, optimal control algorithms for multistage optimization have been applied to obtain a robust solution.

For both reactor configurations, the stirred and the tubular configuration, the developed optimization approach yields promising results. For the stirred configuration, the side feed turns out to be an important variable to control the SE, since it contributes to the mixture inside the CSTR, forming a more homogeneous polymer. Besides, combinations of extremely low SE and MI show to have less economic benefit due to low catalyst consumption and high ethylene use. For the tubular configuration, the importance of hydrogen as

Table 11. Industrial Practice vs. Optimal Operating Conditions

Variables		Industrial Practice	Optimum	
			Scenario 1	Scenario 2
Decision variable	CAT	0.769	0.896	0.896
	M	0.717	0.750	0.750
	H_0	0.033	0.049	0.050
	T_{in}	0.325	0.250	0.250
	P_{in}	0.692	1.000	0.987
	W_t	0.600	0.513	0.477
	H_1	0.667	0.173	0.173
	z_1	0.352	0.281	0.277
Quality variable	MI	0.282	0.282	0.282
	SE	0.713	0.713	0.713
	DS	0.925	0.925	0.925
Output variable	T_{out}	0.880	1.000	1.000
	P_{out}	0.563	0.500	0.533
	Q	0.966	0.976	0.976
	W_{PE}	0.605	0.621	0.605
	Revenue	0.663	0.673	0.663
	Cost	0.572	0.564	0.556
	Profit	0.090	0.109	0.107

chain transfer agent and its injection point along the reactor are illustrated. Higher ethylene and catalyst input concentrations can lead to higher profits while the polymer properties are controlled by the hydrogen. Besides, the outlet temperature proves to be an important variable to be controlled in order to drive the process to higher profits. Moreover, a nonlinear behavior is observed for both reactor configurations, i.e., the tendency of the profit profiles vs. SE and MI strongly depends not only on the reactor configuration employed but also on the specified values for the polymer properties.

The mathematical modeling approach for the design of target polymer overcomes several disadvantages of the usual industrial scale experiments. The potential and usefulness of the proposed approach are evidenced through its application to a variety of examples with different polymer grades in a highly nonlinear process. The optimization model developed here is shown to be an attractive tool to support the development of new resins or to improve product quality in the existing production process. It allows for the determination of the optimal operating policies to produce a tailored polyethylene resin, whereas it yields the economically optimal operating condition. It is a versatile tool since other constraints can be easily implemented, the parameters of the objective function can be changed or new terms can be added easily. In addition, other polymerization process models can be used as a basis for the optimization.

Acknowledgments

The authors acknowledge CAPES (Coordenação de Aperfeiçoamento de Pessoal de Nível Superior) and DAAD (Deutscher Akademischer Austauschdienst) for financial support.

Notation

a = polyethylene sales price (€/Kg)
a = constant coefficient
b = unitary costs (€/Kg)
B = recycle stream mass flow rate (Kg/s)
C = catalyst
C_i = component i concentration (kmol/m^3)
C^* = activated catalyst
CC = co-catalyst
CCD = deactivated co-catalyst
CD = deactivated catalyst
$\hat{C}p$ = specific heat (J/Kg K)
D_0, D_{Ror}, D_F = constant coefficient
DS = polymer density
$\mathbf{f}$ = vector of differential equations
F = mass flow rate (Kg/s)
FZ = mass flow rate (Kg/s)
$\mathbf{g}$ = vector of algebraic equations
H_0 = hydrogen concentration at main feed
H_j = hydrogen concentration at lateral injection point
ΔH_p^o = enthalpy of reaction at the reference temperature (J/kmol)
I = poison
$\mathbf{J}$ = vector of mapping conditions
k = constant coefficient
k = stage number
$k_{f'}$ = rate constant for activation
$k_{iCC'}$ = rate constant for co-catalyst poisoning
$k_{iC^{*'}}$ = rate constant for catalyst poisoning
k_i = rate constant for initiation
k_p = rate constant for propagation
k_{fm} = rate constant for transfer with monomer
k_{fh} = rate constant for transfer with hydrogen
k_{fCC} = rate constant for transfer with co-catalyst
k_f = rate constant for spontaneous transfer
k_d = rate constant for spontaneous deactivation
k_{tm} = rate constant for termination with monomer
k_{th} = rate constant for termination with hydrogen
k_{tCC} = rate constant for termination with co-catalyst
k_t = rate constant for spontaneous termination
$\mathbf{lb}$ = vector of lower bounds
M = monomer
MI = polymer Melt Index
MW = molecular weight
$\overline{MW}_n$ = polymer numerical molecular weight
$\overline{MW}_w$ = polymer weight molecular weight
nc = number of components
nk = number of modes or stages
$\mathbf{p}$ = vector of time invariant parameters
P = live polymer
ΔP = pressure drop
PD = polydispersity
P_{in} = inlet pressure
P_{out} = outlet pressure
Q = conversion
r = reaction rate
Rot = agitator rotation
SE = polymer stress exponent
t = time
T = temperature
T_{in} = inlet temperature
T_{out} = outlet temperature
U = dead polymer
$\mathbf{u}$ = vector of control variables
$\mathbf{ub}$ = vector of upper bounds
V = volume (m^3)
W = mass flow rate (Kg/s)
W_{PE} = polymer production rate
W_s = side feed
W_t = total mass flow rate
$\boldsymbol{x}$ = vector of differential state variables
$\boldsymbol{y}$ = vector of algebraic state variables
z = axial coordinate
z_j = lateral hydrogen injection point

Subscripts

s = reactor agitated configuration
C = component concentration
C^* = activated catalyst
e = input
i = component
M = monomer
n = active catalyst site type
p = polymer chain length
p = propagation reaction
r = CSTR ideal zone
t = reactor tubular configuration
U = dead polymer

Superscript

ne = number of input streams

Greek letters

α, β, γ, δ = empirical constants
τ, ξ, K = empirical constants
λ_k = dead polymer moment of order k
μ = polymer viscosity
ρ = medium specific mass (Kg/m^3)
τ = tensor (N/m^2)
v = fluid velocity (m/s)

Literature Cited

1. Louie BM, Soong DS. Optimization of batch polymerization processes—narrowing the MWD. I. Model simulation. *J Appl Polym Sci*. 1985;30:3707–3749.

2. Chen SA, Lee ST. Minimum end time policies for batch-wise radical chain polymerization. V. Multicomponent copolymerization with one-charge of comonomer. *Polym Eng Sci*. 1985;25:987–1000.
3. Chen SA, Lee ST. Minimum end time policies for batch-wise radical chain polymerization. VI. The initiator addition policies for copolymerization with constant copolymer composition control. *Polym Eng Sci*. 1987;27:573–581.
4. Ponnuswamy SR, Shah SL. Computer optimal control of batch polymerization reactors. *Ind Eng Chem Res*. 1987;26:2229–2236.
5. Choi KY, Butala DN. An experimental study of multiobjective dynamic optimization of a semibatch copolymerization process. *Polym Eng Sci*. 1991;31:353–364.
6. Vaid NR, Gupta SK. Optimal temperature profiles for methylmetacrylate polymerization in the presence of end point constraints. *Polym Eng Sci*. 1991;31:1708–1715.
7. Tieu D, Cluett R, Penlidis A. Optimization of polymerization reactor operation: review and case studies with the end-point collocation method. *Polym React Eng*. 1994;2:275–313.
8. Secchi AS, Lima EL, Pinto JC. Constrained optimal batch polymerization reactor control. *Polym Eng Sci*. 1990;30:1209–1219.
9. Ahn AO, Chang SC, Rhee HK. Application of optimal temperature trajectory to batch polymerization reactor. *J Appl Polym Sci*. 1998; 69:59–68.
10. Hanai T, Ohki T, Honda H, Kobayashi T. Analysis of initial conditions for polymerization reaction using fuzzy neural network and genetic algorithm. *Comput Chem Eng*. 2003;27:1011–1019.
11. Chakravarthy SSS, Saraf DN, Gupta SK. Use of genetic algorithms in the optimization of free radical polymerizations exhibiting the trommsdorff effect. *J Appl Polym Sci*. 1997;63:529–548.
12. Oliveira AT, Biscaia EC, Pinto JC. Optimization of batch solution polymerizations: simulation studies using an inhibitor and a chain-tansfer agent. *J Appl Polym Sci*. 1998;69:1137–1152.
13. Ray AK, Gupta SK. Optimization of nonvaporizing nylon 6 reactors with stopping conditions and end-point constraints. *Polym Eng Sci*. 1986;26:1033–1044.
14. Srivastava D, Gupta SK. Optimization of a tubular nylon 6 reactor with radial gradients. *Polym Eng Sci*. 1991;31:596–606.
15. Scali C, Ciari R, Bello T, Maschio G. Optimal temperature for the control of the product quality in batch polymerization: simulation and experimental results. *J Appl Polym Sci*. 1995;55:945–959.
16. Brandolin A, Valles EM, Farber JN. High pressure tubular reactors for ethylene. Polymerization optimization aspects. *Polym Eng Sci*. 1991;31:381–390.
17. Zhou F, Gupta SK, Ray AK. Multiobjective optimization of the continuous casting process for poly(methylmetacrilate) using adapted genetic algorithm. *J Appl Polym Sci*. 2000;78:1439–1458.
18. Faliks A, Yetter RA, Foudas CA, Wie Y, Rabitz H. Optimization of polymer synthesis through distributed control of polymerization conditions. *J Appl Polym Sci*. 2002;85:2922–2928.
19. Lemoine-Nava R, Flores-Tlacuahauc A. Optimal operating policies for the nitroxide-mediated radical polymerization of styrene in a semibatch reactor. *Ind Eng Chem Res*. 2006;45:4637–4652.
20. O'Driscoll KF, Ponnuswamy SR. Optimization of a batch polymerization reactor at the final stage of conversion. II. Molecular weight constraint. *J Appl Polym Sci*. 1990;39:1299–1308.
21. Fernandes FAN, Lona LMF, Penlidis A. Inverse modeling applications in emulsion polymerization of vinyl acetate. *Chem Eng Sci*. 2004;59:3159–3167.
22. Curteanu S. Direct and inverse neural network modeling in free radical polymerization. *Central Eur J Chem*. 2004;2:113–140.
23. Gosden RG, Sahakaro K, Johnson AF, Chen J, Li RF, Wang XZ, Meszena ZG. Living polymerization reactors: molecular weight distribution control using inverse neural network models. *Polym React Eng*. 2001;9:249–270.
24. Asteasuain M, Ugrin PE, Lacunza MH, Brandolin A. Effect of multiple feedings in the operation of a high-pressure polymerization reactor for ethylene polymerization. *Polym React Eng*. 2001;9:163–182.
25. Brandolin A, Lacunza MH, Ugrin PE, Capiati NJ. High pressure polymerization of ethylene. An improved mathematical model for industrial tubular reactors. *Polym React Eng*. 1996;4:193–241.
26. Zabisky RCM, Chan WM, Gloor PE, Hamielec AW. A kinetic model for olefin polymerization in high-pressure tubular reactors: a review and update. *Polymer*. 1992;33:2243–2262.
27. Carvalho AB, Gloor PE, Hamielec AE. A kinetic mathematical model for heterogeneous Ziegler-Natta copolymerization. *Polymer*. 1989;30:280–296.
28. McAuley KB, MacGregor JF, Hamielec AE. A kinetic model for industrial gas-phase polyethylene copolymerization. *AIChE J*. 1990; 36:837–850.
29. Xie TY, McAuley KB, Hsu JCC, Bacon DW. Gas phase ethylene polymerization: production process, polymer properties, and reactor modeling. *Ind Eng Chem Res*. 1994;33:449–479.
30. Fontes CH, Mendes MJ. Analysis of an industrial continuous slurry reactor for ethylene-butene copolymerization. *Polymer*. 2005;46: 2922–2932.
31. Mattos Neto AG, Freitas MF, Nele M, Pinto JC. Modeling ethylene/1-butene copolymerizations in industrial slurry reactors. *Ind Eng Chem Res*. 2005;44:2697–2715.
32. Kim KJ, Choi KY. Continuous olefin copolymerization with soluble Ziegler-Natta catalysts. *AIChE J*. 1991;37:1255–1260.
33. Cozewith C. Transient response of continuous-flow stirred-tank polymerization reactors. *AIChE J*. 1988;34:272–282.
34. Embiruçu M, Lima EL, Pinto JC. Continuous soluble Ziegler-Natta ethylene polymerizations in reactor trains. I. Mathematical modeling. *J Appl Polym Sci*. 2000;77:1574–1590.
35. Hinchliffe M, Montague G, Willis M. Hybrid approach to modeling an industrial polyethylene process. *AIChE J*. 2003;49:3127–3137.
36. Embiruçu M, Prata DM, Lima EL, Pinto JC. Continuous soluble Ziegler-Natta ethylene polymerizations in reactor trains. II. Estimation of kinetic parameters from industrial data. *Macromol React Eng*. 2008;2:142–160.
37. Xie TY, McAuley KB, Hsu JCC, Bacon DW. Modeling molecular-weight development of gas-phase a-olefin copolymerization. *AIChE J*. 1995;41:1251–1265.
38. Galvan R, Tirrell M. Distribution predictions for heterogeneous Ziegler-Natta polymerization using a two-site model. *Chem Eng Sci*. 1986;41:2385–2393.
39. Chan WM, Gloor PE, Hamielec AE. A kinetic model for olefin polymerization in high-pressure autoclave reactors. *AIChE J*. 1993;39: 111–126.
40. Marini L, Georgakis C. Low-density polyethylene vessel reactors. I. Steady state and dynamic modelling. *AIChE J*. 1984;30:401–408.
41. Tosun G. A mathematical model of mixing and polymerization in a semibatch stirred-tank reactor. *AIChE J*. 1992;38:425–437.
42. Osswald T, Hernández-Ortiz JP. *Polymer Processing, Modeling and Simulation*, *1st ed*. Germany: Hanser, 2006.
43. Anonymous. *SclairTech Process Technology Manual*. Canada: Du Pont, 1989.
44. Gahleitner M, Wolfschwenger J, Bachner C, Bernreitner K, Neibl W. Crystalinity and mechanical properties of pp-homopolymers as influenced by molecular structure and nucleation. *J Appl Polym Sci*. 1996;61:649–657.
45. Kiashemshaki A, Mostoufi N, Sotudeh-Gharebagh R, Pourmahdian S. Reactor modeling of gas-phase polymerization of ethylene. *Chem Eng Technol*. 2004;27:1227–1232.
46. Kumar A, Gupta RK. *Fundamentals of Polymers*. New York: McGraw-Hill, 1998.
47. Embiruçu M, Pontes K, Lima EL, Pinto JC. Continuous soluble Ziegler-Natta ethylene polymerizations in reactor trains. III. Influence of operation conditions upon process performance. *Macromol React Eng*. 2008;2:161–178.
48. Vassiliadis VS, Sargent RWH, Pantelides CC. Solution of a class of multistage dynamic optimization problems. 1. Problems without path constraints. *Ind Eng Chem Res*. 1994;33:2111–2122.
49. Cruse A, Marquardt W, Oldenburg J, Schlegel M. Batch process modeling and optimization. In: Korovessi E, Linninger A, editors. *Batch Processes, Chemical Industries*. Boca Raton, FL: CRC Press, 2005:305–387.
50. Barton PI, Allgor RJ, Feehery WF, Galán S. Dynamic optimization in a discontinuous world. *Ind Eng Chem Res*. 1998;37:966–981.
51. Brendel M, Oldenburg J, Schlegel M, Stockmann K. *Dyos user manual, relase 2.1. Lehrstuhl für Prozesstechnik*, RWTH Aachen, Aachen, Germany, 2002.
52. Oldenburg J, Marquardt W. Disjunctive modeling for optimal control of discrete-continuous dynamic systems. *Comp Chem Eng*. In Press, doi:10.1016/j.compchemeng.2007.12.002.

53. Binder T, Blank L, Bock HG, Bulirsch R, Dahmen W, Diehl M, Kronseder T, Marquardt W, Schlöder JP, von Stryk O. Introduction to model based optimization of chemical processes on moving horizons. In: Grötschel M, Krumke SO, Rambau J, editors. *Online Optimization of Large Scale Systems*. Berlin, Heidelberg: Springer-Verlag, 2001:297–339.
54. Gill, PE, Murray W, Saunders A. *User's guide for SNOPT 5.3: a Fortran package for large-scale nonlinear programming*. Technical Report, California, USA, 1997.
55. Schlegel M, Marquardt W, Ehrig R, Nowak U. Sensitivity analysis of linearly-implicit differential-algebraic systems by one-step extrapolation. *Appl Num Math*. 2004;48:83–102.
56. Witney JR, Wilson RE, Wicks CE. *Fundamentals of Momentum, Heat and Mass Transfer*, *2nd ed*. New York: Wiley, 1976.
57. Bird RB, Stewart WE, Lightfoot EN. *Transport Phenomena*. New York: Wiley, 1960.
58. Marquardt W. Towards a process modeling methodology. In: Berber R, editor. *Methods of Model Based Process Control*. Dordrecht, The Netherlands: Kluwer, 1995:3–40.

Appendix

This appendix presents the development of the mass and energy balances for a tubular reactor, which operates in turbulent flow. There are no variations on the radial and azimuthal coordinates, hence only the axial coordinate is considered.

The general mass balance may be written as[56,57]

$$\frac{\partial \rho}{\partial t} + \nabla \cdot (\rho \mathbf{v}) = 0, \tag{A1}$$

where ρ is the density of the mixture (kg/m^3) and $\boldsymbol{v}$ is the velocity of the fluid (m/s). For steady-state operation of the considered PFR reactor, this equation reduces to

$$\frac{\partial(\rho \cdot v_z)}{\partial z} = 0 \Leftrightarrow \frac{\partial v_z}{\partial z} = -\frac{v_z}{\rho} \cdot \frac{\partial \rho}{\partial z}. \tag{A2}$$

The fluid velocity is defined as $W/(\rho \cdot A)$, where W is the mass flow rate (kg/s), ρ is the density of the mixture (kg/m^3), and A is the cross-sectional area (m^2), which is constant. Introducing this definition into Eq. A2 results in

$$\frac{1}{A} \cdot \frac{\partial W}{\partial z} = 0. \tag{A3}$$

The continuity equation for a component i, in mass basis, is given by

$$\nabla(\rho_i \mathbf{v}) + \frac{\partial \rho_i}{\partial t} - r_i^* = 0, \quad i = 1, \ldots, nc, \tag{A4}$$

where ρ_i is the mass concentration of component i (kg/m^3), defined as $\rho_i = w_j \cdot \rho$, where ρ is the mixture density (kg/m^3) and w_i is the mass fraction of component i, r_i^* is the reaction rate of component i (kg/m^3 s), nc is the number of components and $\boldsymbol{v}$ is the fluid velocity (m/s). For the studied PFR and introducing the definition of ρ_i, given above,

$$w_i \cdot \frac{\partial(\rho \cdot v_z)}{\partial z} + \rho \cdot v_z \cdot \frac{\partial w_i}{\partial z} = r_i^* \tag{A5}$$

With Eq. A2, this equation may be rewritten to the component mass balance

$$\rho \cdot v_z \cdot \frac{\partial w_i}{\partial z} = r_i^* \tag{A6}$$

Using the definition $C_i = \rho_i/M_i$ in Eq. A4, where M_i is the molecular weight of component i, it is possible to write the component mass balance in molar basis, according to:

$$M_i \cdot v_z \cdot \frac{\partial C_i}{\partial z} + C_i \cdot M_i \cdot \frac{\partial v_z}{\partial z} = r_i^* \tag{A7}$$

Inserting Eq. A2 into Eq. A7 results in

$$\frac{\partial C_i}{\partial z} = \frac{C_i}{\rho} \cdot \frac{\partial \rho}{\partial z} + \frac{r_i}{v_z} \Leftrightarrow \frac{\partial C_i}{\partial z} = \frac{C_i}{\rho} \cdot \frac{\partial \rho}{\partial z} + r_i \cdot \frac{\rho \cdot A}{W} \tag{A8}$$

where r_i is the reaction rate of component i (mol/m^3 s) and Eq. A8 is the component mass balance in molar basis.

The general energy balance for a PFR is given by[57,58]

$$\frac{\partial \rho h}{\partial t} + \nabla(\rho h \mathbf{v}) + \nabla \mathbf{q} = \frac{\partial P}{\partial t} - (\tau : \nabla \mathbf{v}) + (\mathbf{v} \cdot \nabla \mathbf{P}) \tag{A9}$$

where ρ is the mixture density (kg/m3), h is the mixture specific enthalpy (J/kg), $\boldsymbol{q}$ is the conduction heat (J/s m^3), P is pressure (N/m^2), $\boldsymbol{v}$ is the fluid velocity (m/s) and the two last terms on the right hand side are the energy contributions by viscous friction and by reversible effects. For the steady state PFR under consideration, there are no conduction effects. Because of the turbulent flow, the viscosity effects may be neglected and it is assumed that the pressure gradient can be neglected. Bearing this is mind, Eq. A9 may be rewritten to

$$\rho v_z \cdot \frac{\partial h}{\partial z} + h \cdot \frac{\partial(\rho v_z)}{\partial z} = 0. \tag{A10}$$

With Eq. A2 we obtain

$$\rho v_z \cdot \frac{\partial h}{\partial z} = 0 \Rightarrow \frac{\partial h}{\partial z} = 0. \tag{A11}$$

The total enthalpy of a mixture (H, J) is given by the specific partial enthalpies $\bar{h}_i$(J/kg) according to

$$H = M \cdot h = M \cdot \sum_{i=1}^{nc} w_i \bar{h}_i \tag{A12}$$

Introducing this equation into Eq. A11, we get

$$\frac{\partial \sum_{i=1}^{nc} w_i \bar{h}_i}{\partial z} = \sum_{i=1}^{\mathrm{nc}} w_i \cdot \frac{\partial \bar{h}_i}{\partial z} + \sum_{i=1}^{\mathrm{nc}} \bar{h}_i \cdot \frac{\partial w_i}{\partial z} = 0 \tag{A13}$$

From the definition of the partial specific heat $\overline{C}\mathrm{p}_i$ of component i (J/kg K) and from Eq. A6, we get

$$\frac{W \cdot C\mathrm{p}}{A} \cdot \frac{\partial T}{\partial z} = -\sum_{i=1}^{nc} \bar{h}_\mathrm{i} \cdot r_i^* \tag{A14}$$

where Cp is the specific heat of the mixture (J/Kg K).

The heat released by the polymerization reaction is mainly due to propagation reactions. Besides, the specific heat of the polymer is independent of the chain length. With this assumption, the final energy balance equation for the PFR is given by

$$\frac{W}{A}\cdot\frac{\partial T}{\partial z}=-\frac{r_{\mathrm{p}}}{C\mathrm{p}}\cdot\left(\Delta\bar{H}_{\mathrm{p}}^{o}+\mathrm{MW_M}\cdot\int_{To}^{Tr}(\mathrm{Cp_U}-\mathrm{Cp_M})dT\right) \quad \text{(A15)}$$

where $C\mathrm{p_U}$ and $C\mathrm{p_M}$ are the specific heats (J/kg K) ofpolymer and monomer, $\mathrm{MW_M}$ is the molecular weight of the monomer (kg/kmol), r_{p} is the rate of the propagation reaction (kmol/s m^3), $\Delta\overline{\mathrm{H}}_{\mathrm{p}}^{o}$ is the enthalpy of this reaction at the reference temperature (J/kmol), T^r is the reaction temperature, T^i is the input temperature and T^{o} is the reference temperature.

Manuscript received Sept. 28, 2007, and revision received Apr. 15, 2008.